THE JOURNAL OF CHEMICAL PHYSICS

VOLUME 11 NUMBER 9

SEPTEMBER, 1943

Published by the

AMERICAN INSTITUTE OF PHYSICS

Incorporated

LANCASTER, PA., AND NEW YORK, N. Y.

THE JOURNAL OF CHEMICAL PHYSICS

ADVISORY EDITORIAL BOARD

R. T. BIRGE
A. H. COMPTON
JAMES FRANCK
IRVING LANGMUIR
JOHN T. TATE
HAROLD C. UREY

BOARD OF EDITORS

JOSEPH E. MAYER, *Editor*

Associate Editors

Term ending December 31, 1945
SIMON FREED
MAURICE L. HUGGINS
J. G. KIRKWOOD
GEORGE SCATCHARD
J. H. VAN VLECK

Term ending December 31, 1944
CHARLES O. BECKMAN
BRYCE L. CRAWFORD, JR.
P. DEBYE
DAVID HARKER
FRANK H. WESTHEIMER

Term ending December 31, 1943
L. O. BROCKWAY
RONALD W. GURNEY
KENNETH S. PITZER
ALFRED L. SKLAR
E. W. R. STEACIE
HUGH S. TAYLOR

THE JOURNAL OF CHEMICAL PHYSICS is published monthly by the American Institute of Physics. Its purpose is to bridge a gap between journals of physics and journals of chemistry. The artificial boundary between physics and chemistry has now been in actual fact completely eliminated, and a large and active group is engaged in research which is as much the one as the other. It is to this group that the Journal is rendering its principal service and makes its greatest appeal, both as a prompt and efficient medium for publication of research and as a convenient and carefully edited assemblage of pertinent information.

Manuscripts for publication should be submitted to Joseph E. Mayer, Havemeyer Hall, Columbia University, New York 27, New York.

Proof and all correspondence concerning papers in the process of publication should be addressed to the Publications Manager, American Institute of Physics, 175 Fifth Avenue, New York 10, New York.

Subscriptions and orders for single copies should be addressed to Prince and Lemon Streets, Lancaster, Pennsylvania, or to the American Institute of Physics, 175 Fifth Avenue, New York 10, New York.

Changes of address should be addressed to the Publications Manager.

Subscription Price

The United States and Possessions, Canada and Mexico $10.00
Elsewhere 11.00

Back Numbers

Complete set: Vol 1, 1933—Vol 10, 1942 ..... $100.00
Yearly rate: $11.00.
Single copies: $1.00 each.

The Journal of Chemical Physics is published monthly at Prince and Lemon Streets, Lancaster, Pennsylvania.

Entered as second-class matter December 30, 1932, at the Post Office at Lancaster, Pa., under the Act of August 24, 1912. Acceptance for mailing at special rate of postage, provided for in the Act of February 28, 1925, embodied in paragraph 4, Section 538, P. L. & R.: authorized February 3, 1933.

THE JOURNAL
OF
CHEMICAL PHYSICS

VOLUME 11, NUMBER 9 SEPTEMBER, 1943

Equilibrium in Hydrogen-Water Systems Containing Tritium

JAMES F. BLACK AND HUGH S. TAYLOR
Frick Chemical Laboratory, Princeton University, Princeton, N. J.
(Received June 8, 1943)

The equilibrium constant of the reaction $HT+H_2O=H_2+HTO$ involving radioactive hydrogen (T) has been determined over the temperature range 289 to 576°K in contact with a platinum-charcoal catalyst. The results are summarized in the equations:

$$\log K=0.292 \log T+336.5/T-1.055$$
$$\Delta F^\circ=+4.83T-1.34T \log T-1540$$
$$\Delta H^\circ=0.58T-1540$$
$$\Delta S^\circ=1.34 \log T-4.25$$
$$\Delta C_p^\circ=0.58\pm0.05 \text{ cal./deg./mole}$$
$$\Delta H_o^\circ=-1540\pm160 \text{ cal./mole}$$
$$I=1.055.$$

Comparison of the experimental results with theoretical calculations by W. F. Libby indicates the correctness of these latter and confirms the assumption with respect to isotopic species that the forces acting within a molecule are unaltered by the change in nuclear mass and that any effects on the properties of the molecule are solely due to a different mass moving in the same force field.

THE object of these experiments is the determination of the equilibrium constant of the reaction HT+HHO=HH+HTO, "T" being "tritium," the hydrogen isotope of mass 3, first detected in 1934.[1] The equilibrium can be followed by virtue of the radioactivity of tritium[2] which is evidenced by a weak beta-radiation with a half-life of 31±8 years.[3]

The interest in this determination lies in the effect of isotopic substitution upon the potential function of a molecule. The usual assumption of this effect is that the forces acting within the molecule are unaltered by the change in nuclear mass and that any effects upon the properties of the molecule are solely due to a different mass moving in the same force field. On the basis of this assumption, calculations have been made by W. F. Libby[4] of the equilibrium constant of the reaction investigated in this report. This reaction is simple enough for accurate theoretical treatment and is concerned with a mass difference which should provide the best possible criterion of the assumptions involved concerning isotopes.

EXPERIMENTAL METHOD

The equilibrium constant determined here is written $(HTO)(HH)/(HT)(HHO)=K$. Alter-

[1] Oliphant, Harteck, and Rutherford, Nature **133**, 413 (1934).
[2] Luis W. Alvarez and Robert Cornog, Phys. Rev. **56**, 613 (1939).
[3] R. D. O'Neal and M. Goldhaber, Phys. Rev. **58**, 574–5 (1940).
[4] W. F. Libby, J. Chem. Phys. **11**, 101 (1943).

nately, this may be put

$$\frac{(\mathrm{HTO})/(\mathrm{HHO})}{(\mathrm{HT})/(\mathrm{HH})}=K,$$

which is the form into which substitution was made in these experiments.

The partial pressure of HTO (or of HT) in a given container is proportional to the number of disintegrations resulting from it per minute. In a sample of radioactive water or hydrogen which will give a convenient counting rate, however, the actual mole fraction of tritium present is of the order of 10^{-12} so that the total pressure of a sample of radioactive hydrogen or water vapor may very safely be used as the partial pressure of the inactive species. Therefore, after equilibrium has been established, by separating the hydrogen, active plus inactive, from the water vapor, active plus inactive, and putting each in turn into the same counter where the counts per minute and the pressure to which the sample had been introduced were noted, we could write counts per minute per cm Hg for water vapor (kHTO/HHO) over counts per minute per cm Hg for hydrogen (kHT/HH) to obtain the desired constant.

The first problem was to obtain equilibrium. This was done for the runs at 16°C, 20°C and 25°C by placing the platinum on carbon catalyst within a water-jacketed condenser. Constant temperature was maintained by running water from a thermostat through the water jacket. The radioactive water was placed immediately on the catalyst with the hydrogen being cycled over it and around a closed system until equilibrium had been reached. A portion of the system, enclosing a sample of the equilibrated hydrogen and water vapor, was now shut off. No further change would occur within this sample since the exchange of hydrogen isotopes between hydrogen and water is not catalyzed by glass.[5] The two gases were separated by freezing out the water vapor with a cold bath, after which each could be counted separately.

For the runs above 25°C, a very active catalyst was used. This was kept at constant temperature in a vapor bath. The inactive hydrogen was bubbled through radioactive water, held at constant temperature, and the mixture passed over the catalyst, where equilibrium was established. It then flowed on through a sample trap where a sample could be closed off and analyzed as in the previous apparatus.

In both these methods it is important that a sample of hydrogen and water *vapor*, in equilibrium, was obtained. Thus, the gaseous equilibrium was investigated. To do this it was necessary to be very careful that none of the water vapor was removed by condensation after equilibrium had been established. Such an occurrence would result in a concentration of tritium within the condensed phase, due to the extreme isotopic effect between tritium and hydrogen, and a constant below the true value would result.

The counting was carried out in a Geiger-Mueller tube counter of one-liter volume. The counting mixture was composed of 0.2-cm water vapor, 2.5-cm alcohol, from 0.8- to 2.0-cm hydrogen and 2.0-cm argon. This mixture was always introduced in the same order, the pressures being measured by a closed-end manometer which was utilized as a McLeod gauge to read the water vapor pressure when that gas was the active material. The tube, so filled, had a plateau (region where the count is independent of the wall voltage) about 20 volts long with a center about 50 volts above the threshold (the wall voltage at which counts first can be detected). In each count, we tried to set the voltage so that the tube would be operating at the center of the plateau, where reproducibility is most easily obtained.

Initially, it was necessary to check the reproducibility of the counting conditions by bringing a standard uranium sample to an exact position near the counter and noting the number of counts per minute it produced in addition to the count being determined. This latter was then corrected by the factor necessary to bring this additional number of counts to a standard value.

This method was used for the first four runs at 20°C, which was the first temperature investigated. For the rest of the runs, however, such a correction was not employed, since it was

[5] Gould, Bleakney, and Taylor, J. Chem. Phys. 2, 362 (1934).

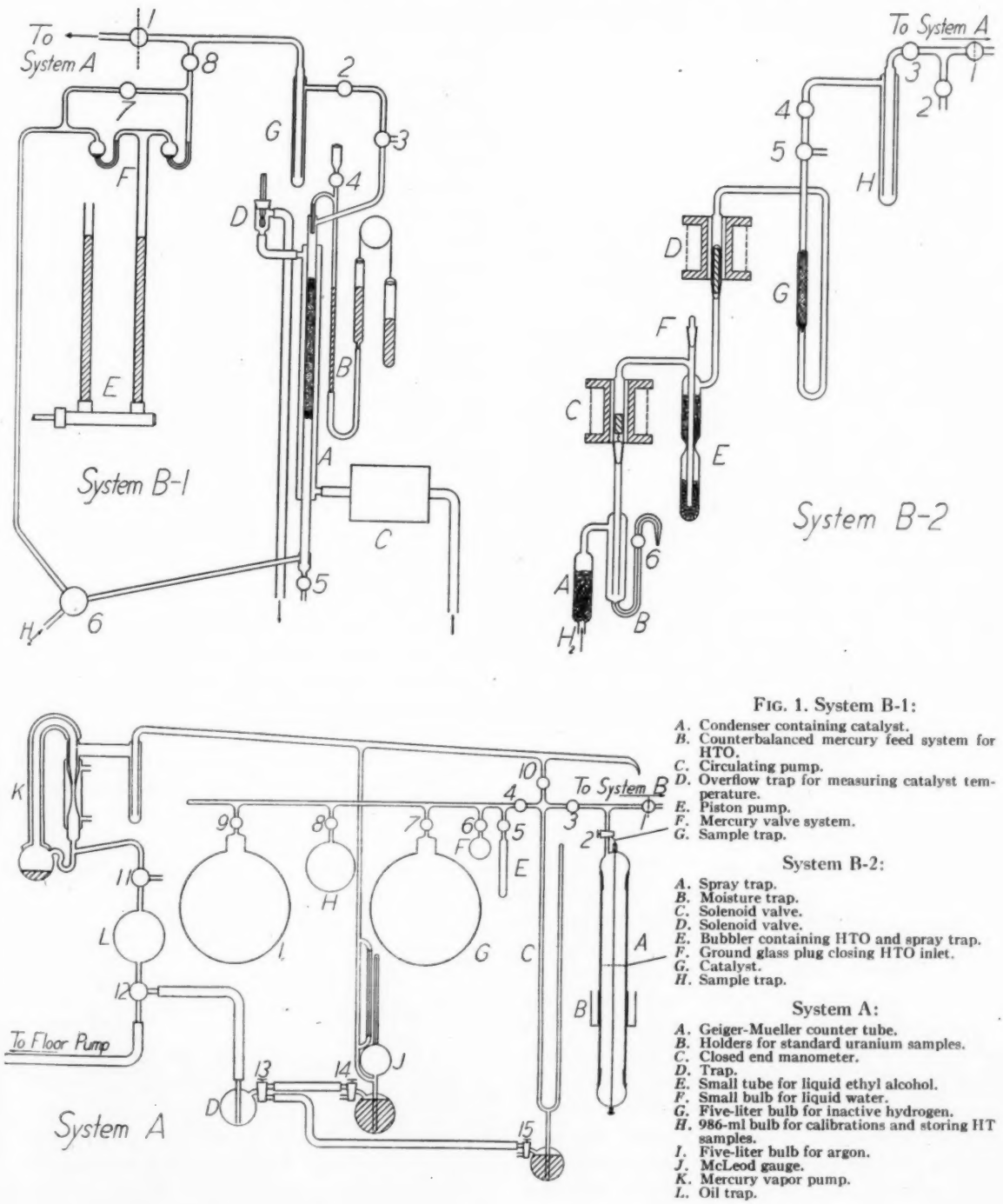

FIG. 1. System B-1:

A. Condenser containing catalyst.
B. Counterbalanced mercury feed system for HTO.
C. Circulating pump.
D. Overflow trap for measuring catalyst temperature.
E. Piston pump.
F. Mercury valve system.
G. Sample trap.

System B-2:

A. Spray trap.
B. Moisture trap.
C. Solenoid valve.
D. Solenoid valve.
E. Bubbler containing HTO and spray trap.
F. Ground glass plug closing HTO inlet.
G. Catalyst.
H. Sample trap.

System A:

A. Geiger-Mueller counter tube.
B. Holders for standard uranium samples.
C. Closed end manometer.
D. Trap.
E. Small tube for liquid ethyl alcohol.
F. Small bulb for liquid water.
G. Five-liter bulb for inactive hydrogen.
H. 986-ml bulb for calibrations and storing HT samples.
I. Five-liter bulb for argon.
J. McLeod gauge.
K. Mercury vapor pump.
L. Oil trap.

found possible to keep the sensitivity actually more constant than the accuracy in this method of determining it.

To get accurate comparisons at the high counting rates involved in these experiments a coincidence correction was employed. This gave, at a given counting rate, the number of counts per minute that had followed too closely after the preceding count for the apparatus to record them both.

APPARATUS AND PROCEDURE

The experiments were performed in two different sets of apparatus shown in Fig. 1.

System A comprises the evacuating devices, counter tube, measuring devices and storage bulbs. These pieces of equipment were maintained as shown throughout the entire series of runs. At the point marked by the inscription "to system B" and by the arrow, system A was sealed to the apparatus in which equilibrium was obtained.

It was in this latter part of the apparatus that two different techniques were involved. The first method, depicted as "system B-1," was used to obtain equilibrium at 16°C, 20°C and 25°C. For higher temperatures, the equipment shown in "system B-2" was employed. Both of these apparatus were joined to system A at the "sample trap," the stopcock labeled "1" and divided by the dotted line being common to both systems A and B in each case.

The auxiliary electrical apparatus necessary for the use of the counter tube in system A was contained in a high speed, Geiger-Mueller counting unit purchased from Herbach and Rademan, Inc.

System B-1

Investigations were first carried out in system B-1. The catalyst was contained in the inner tube of the water-jacketed condenser (*A*). The radioactive water was introduced into the feed system (*B*) through stopcock 4 by lowering the mercury level within the feed system.

The catalyst, kept in good thermal contact with the walls by means of the excess water wetting them both, was held at constant temperature by water from a thermostat. A circulating pump (*C*) forced the water through the outer jacket of the condenser, returning it through the overflow trap (*D*) where the temperature was measured by a thermometer. It was necessary to keep the temperature of the room above that of the catalyst to prevent radioactive water from distilling out of that part of the system.

The hydrogen, generated electrolytically, was passed over platinized asbestos to remove any oxygen impurity. The water was removed from the resulting gas by means of phosphorus pentoxide, after which stopcock 6 gave access to the reaction system. Within the latter, the hydrogen was cycled for several hours, long enough for the isotopic equilibrium to be complete for gas and water vapor.

The cycling was accomplished by means of the piston pump (*E*) and mercury valve system (*F*) shown in the drawing. Each of the two identical mercury valves consisted of a bulb connected to capillary tubing and containing a small amount of mercury. Alternating contraction and expansion of the volume between the valves was produced continually by the piston pump which set the mercury columns into oscillation. With stopcock 7 closed, this resulted in a transfer of gas through the valves from right to left. Since the valves formed part of the closed tubular system containing the catalyst, a continuous transfer of gas around the system was accomplished.

Stopcock 7 was inserted for use in filling the system with hydrogen prior to a run. At such a time the sample trap (*G*) was practically empty because of removal of the sample for counting. Since the apparatus operated at atmospheric pressure, an amount of hydrogen corresponding to the sample removed was inserted. The system, after initially being filled with hydrogen, was so operated that no foreign gases were admitted and only the hydrogen removed as a sample in the previous run had to be replaced to commence a new experiment.

System B-2

The equilibrium was studied at temperatures higher than that of the room by means of system B-2.

The hydrogen was generated electrolytically at about one liter per hour with 2.4 amperes current. The generated gas traversed a spray trap (*A*), and then a liquid-air trap (*B*) to dry it completely. The water collected in the latter could be forced out through the capillary tubing leading to stopcock 6.

The gas next traversed solenoid valve (*C*) which separated the active water from the inactive water when the system was not in operation. Beyond this the hydrogen entered the bubbler (*E*), passing down through the long

center tube and bubbling through the glass beads, covered with radioactive water, at the bottom. The radioactive water was added by removing the ground glass tapered plug (*F*) at the bend just above the bubbler. The hydrogen, saturated with radioactive water, next passed through glass wool in the upper half of the bubbler to remove spray. The entire bubbler, including the spray trap, was immersed in a water bath kept at constant temperature in a large Dewar flask.

Traversing solenoid valve (*D*), the gas was introduced into the section heated by the vapor bath and containing the catalyst (*G*). Here it was brought to temperature by passing downward through six-millimeter tubing in which numerous indentations had been punched to facilitate heat exchange. Rounding the bottom "U" of the tube, the mixture of hydrogen and radioactive water vapor passed upward over the catalyst where equilibrium was established.

Passing through stopcock 5, the mixture, now at equilibrium, could either be run out at the exit tube or sent into the sample trap (*H*) through stopcock 4 which was inserted to prevent placing stopcock 5 under the high vacuum sometimes present in the sample trap. The gas left the sample trap via stopcocks 3 and 2, stopcock 1 being closed.

System A

This part of the apparatus was used as depicted throughout the whole series of measurements. It contained the counter tube, storage bulbs, pressure measuring devices, and vacuum equipment. System A was first sealed to system B-1 and later to system B-2, stopcock 1 being the same in all three figures.

The counter tube itself (*A*) was constructed from two-inch o.d. brass tubing one-sixteenth inch thick, and had glass ends. The glass and metal were sealed together with picene wax to give a vacuum-tight container with a volume of about one liter.

Supported very close to but not touching the counter tube wall were the sensitivity holders (*B*). These held two sample tubes of uranium acetate, kept firmly in place in the tube by a layer of paraffin. These tubes were always placed each in the same holder and in exactly the same position as indicated by an arrow on the cork. Thus, they should always give the same number of counts per minute in addition to those being measured inside the counter if other conditions have been reproduced. Their purpose was to check this latter fact.

Gas was admitted to the counter tube through stopcock 2. Stopcock 1 led to the sample trap while stopcock 3 led to the manometer (*C*).

This latter was a closed tube type which could be pulled down by opening stopcocks 12, 13, and 15 to the floor pump. The manometer was used in filling the counter to read the pressures of the gases directly or by the McLeod gauge method. This last was necessary with the radioactive water which was expanded to a pressure of about two millimeters on being introduced into the counter.

Stopcock 4 led to the storage bulbs. Sealed to stopcock 5 was a test tube (*E*) of liquid absolute alcohol, to stopcock 6 a small bulb (*F*) of liquid inactive water, to stopcock 7 a five-liter bulb (*G*) for inactive hydrogen, to stopcock 8 a liter bulb (*H*) for calibration purposes and to store radioactive hydrogen, and to stopcock 9 a five-liter bulb (*I*) of argon. After separation of a sample, the radioactive water vapor was stored in the sample trap which is not shown as part of system A.

Stopcock 10 led to the main vacuum line. A low pressure McLeod gauge (*J*) tapping this line was used to test the efficiency with which the apparatus was being evacuated. The upper end of the main vacuum line was connected to a trap which led into the mercury vapor pump (*K*) backed by a floor pump.

The vacuum system was in continuous operation, since the counter tube had to be evacuating at all times when not in use and for 25 minutes between each individual counting period. Unless the tube were treated to this exhaustive evacuation, the sensitivity would not, in any sense, be reproducible but would depend upon the recent history of the apparatus. The peculiarities in evidence were complex and have not been explained, but the above treatment enabled these measurements to be made with a sensitivity more constant than it was possible to measure.

CALCULATION OF RESULTS

The data which entered immediately into the equilibrium constant were the pressures of HTO and HT samples, the counting rate with these samples and the background counting rate. In the first four runs the counting rates were corrected to a standard sensitivity value of one count per minute.

The constant recorded for each temperature is the average of the successful runs. The constant at 25°C, calculated in this manner, is 6.25 ± 0.05. The error was obtained from the actual deviations of the individual results from the mean. (See Table I.)

INTERPRETATION OF RESULTS

The results of these measurements and their conversion into the form necessary for a plot of $\log K$ against $1/T$ are given in Table II. The plot itself appears in Fig. 2. Such a plot is usually a straight line but, in this case, due to the wide temperature range covered by the experiments, a slight curvature is present.

A plot of the slope against temperature is utilized here to obtain an estimate of ΔC_p. The

TABLE I. Data and results.

Page	Temp. °C	Background	Obs. H Count	Press. H	HT / cm	Obs. HTO Water	Press. Water	HTO / cm	K
Vol. 2									
14	20.2	0.560	1.873	1.46	0.900	2.002	0.251	5.74	6.38
17	20.2	0.583	1.880	1.46	0.888	1.752	0.218	5.36	6.04
20	20.2	0.560	1.915	1.41	0.961	1.715	0.192	6.01	6.25
23	20.2	0.567	1.903	1.46	0.914	1.658	0.199	5.49	6.01
94	20.2	622	1713	1.45	752	1602	0.179	5475	7.28
97	20.2	626	1846	1.48	824	1584	0.181	5300	6.44
100	20.2	610	1795	1.44	823	1556	0.176	5375	6.54
103	20.2	633	1830	1.47	814	1572	0.176	5340	6.55
106	20.2	612	1785	1.48	792	1546	0.168	5560	7.01
109	20.2	622	1889	1.50	844	1536	0.176	5200	6.16
							Av. $K_{20.2}=6.47\pm0.12$		
29	16.0	580	1900	1.48	891	1517	0.140	5980	6.71
32	16.0	588	1900	1.56	841	1323	0.135	5440	6.46
35	16.0	588	1917	1.51	880	1236	0.140	5840	6.63
38	16.0	600	1932	1.57	848	1404	0.140	5745	6.77
46	16.0	603	1764	1.32	879	1460	0.142	6035	6.86
49	16.0	605	1725	1.31	855	1440	0.142	5880	6.88
54	16.0	591	1663	1.27	843	1428	0.148	5655	6.71
58	16.0	596	1690	1.30	841	1367	0.137	5630	6.69
61	16.0	583	1688	1.32	837	1383	0.140	5710	6.82
64	16.0	590	1702	1.33	836	1396	0.143	5640	6.74
67	16.0	585	1640	1.28	825	1386	0.140	5720	6.93
							Av. $K_{16.0}=6.75\pm0.04$		
70	25.0	612	2338	1.99	866	1906	0.238	5440	6.28
73	25.0	616	1824	1.43	845	1894	0.244	5240	6.20
76	25.0	600	1860	1.43	880	1968	0.256	5340	6.07
79	25.0	604	1862	1.45	867	1875	0.233	5450	6.28
82	25.0	620	1955	1.47	907	2199	0.282	5600	6.17
85	25.0	603	1896	1.43	884	2082	0.262	5640	6.38
88	25.0	623	1888	1.44	878	2051	0.256	5580	6.35
							Av. $K_{25.0}=6.25\pm0.05$		
124	56.3	705	1889	1.01	1172	1698	0.169	5870	5.01
127	56.0	625	1860	0.96	1287	1659	0.166	6230	4.84
133	56.0	665	2094	1.00	1429	1739	0.151	7140	4.96
142	56.2	645	2251	1.01	1590	2168	0.196	7770	4.89
145	56.3	669	2036	0.94	1454	1778	0.151	7340	5.04
148	56.1	675	2131	1.00	1456	1802	0.151	7460	5.12
151	55.8	634	2153	0.99	1533	1893	0.158	7960	5.19
154	55.8	665	2282	1.01	1600	1886	0.146	8360	5.22
156	55.5	720	2333	1.02	1582	1991	0.156	8150	5.15
							Av. $K_{56.2}=5.05\pm0.05$		

TABLE I.—*Continued.*

Page	Temp. °C	Background	Obs. H Count	Press. H	HT / cm	Obs. HTO Water	Press. Water	HTO / cm	K
160	79.8	645	2697	0.99	2073	2500	0.213	8700	4.20
162	79.8	631	2474	0.86	2144	2309	0.186	9020	4.21
165	79.6	631	2400	0.81	2184	2335	0.181	9410	4.52
167	79.5	646	2537	0.94	2012	2249	0.173	9260	4.61
169	79.5	663	2524	0.88	2116	2229	0.171	9150	4.32
171	79.2	642	2532	0.89	2124	2603	0.208	9425	4.44
174	79.6	643	2622	0.94	2105	2445	0.198	9090	4.32
175	79.7	643	2452	0.88	2055	2506	0.208	8955	4.36
							Av. $K_{79.6}=4.37\pm0.05$		
177	111.5	676	2585	0.90	2120	2198	0.196	7760	3.66
178	111	673	2460	0.89	2007	2201	0.196	7795	3.88
180	111	673	2367	0.81	2091	2069	0.183	7625	3.65
182	111	671	2334	0.80	2080	2325	0.198	8350	4.01
183	111	671	2537	0.83	2248	2190	0.186	8160	3.63
185	110.0	660	2217	0.80	2217	2255	0.201	7930	3.82
2	111.2	657	2357	0.82	2073	2306	0.208	7925	3.82
4	111.3	657	2365	0.82	2084	2254	0.211	7560	3.63
6	111.2	671	2484	0.83	2185	2618	0.238	8180	3.74
							Av. $K_{111.2}=3.76\pm0.05$		
7	158.7	656	2389	0.82	2115	1973	0.191	6900	3.26
9	158.1	656	2332	0.80	2095	1980	0.196	6750	3.22
10	158.2	656	2358	0.82	2076	1994	0.198	6750	3.25
11	158.2	685	2494	0.81	2232	2020	0.201	6640	2.98
13	158.7	656	2384	0.78	2215	2060	0.226	6210	2.81
15	158.6	656	2542	0.80	2358	2178	0.211	7210	3.06
17	158.4	686	2466	0.80	2225	2121	0.204	7030	3.16
18	158.7	686	2532	0.81	2280	2186	0.208	7200	3.06
							Av. $K_{158.4}=3.10\pm0.06$		
19	216.9	680	2376	0.77	2200	1903	0.204	6000	2.72
21	217.3	680	2483	0.80	2255	1858	0.204	5770	2.56
22	217.3	680	2450	0.81	2185	1836	0.193	5990	2.74
23	217.3	680	2483	0.80	2255	1756	0.186	5785	2.56
24	217.6	664	2653	0.91	2185	1654	0.176	5625	2.58
26	216.5	664	2394	0.77	2247	1815	0.193	5960	2.65
27	217.0	664	2495	0.80	2288	1820	0.181	6390	2.79
28	217.2	664	2643	0.81	2442	1888	0.201	6090	2.50
							Av. $K_{217.1}=2.64\pm0.04$		
30	302.3	660	2545	0.81	2327	1714	0.201	5250	2.26
31	302.3	660	2553	0.81	2338	1720	0.209	5070	2.17
32	303.0	660	2490	0.80	2287	1638	0.188	5200	2.27
33	302.9	660	2600	0.83	2336	1620	0.193	4975	2.13
35	303.6	660	2690	0.86	2360	1611	0.186	5110	2.16
36	303.6	660	2530	0.79	2366	1578	0.186	4935	2.09
37	302.8	660	2698	0.81	2515	1642	0.186	5280	2.10
38	302.1	660	2605	0.81	2400	1627	0.186	5200	2.17
							Av. $K_{302.9}=2.17\pm0.02$		

TABLE II.

t°C	T°K	$1/T$	K	$\log K$	±
16.0	289.1	0.003459	6.75 ± 0.04	0.8293	0.0025
20.2	293.3	3409	6.47 ± 0.12	0.8109	0.0080
25.0	298.1	3354	6.25 ± 0.05	0.7959	0.0034
56.2	329.3	3036	5.05 ± 0.05	0.7033	0.0043
79.6	352.7	2834	4.37 ± 0.05	0.6405	0.0049
111.2	384.3	2602	3.76 ± 0.04	0.5752	0.0051
158.4	413.5	2317	3.10 ± 0.06	0.4914	0.0084
217.1	490.2	2039	2.64 ± 0.04	0.4216	0.0065
302.9	576.0	1736	2.17 ± 0.02	0.3365	0.0040

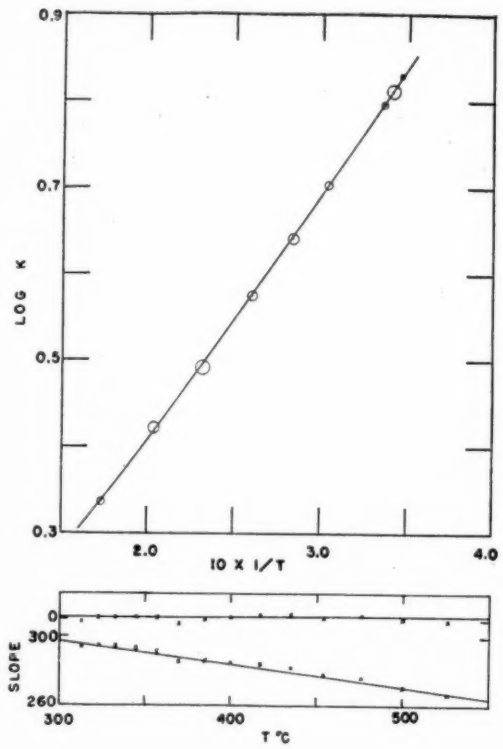

FIG. 2. Upper.
FIG. 3. Lower.

data read from Fig. 2 and the slopes obtained from them are found in Table III. The slopes are plotted against temperature as the lower series of points in the bottom part of Fig. 3. The upper series of points in this section of Fig. 3 represent the deviations of the lower series from the straight line drawn through them. From the two straight lines that are drawn we find the best equation for the data to be slope $=-0.126T+336=(d\log K)/d(1/T)$. Multiplying through by $2.303R$, we obtain

$$2.303R\frac{d\log K}{d(1/T)}=-0.58T+1540. \qquad (1)$$

From Eq. (1) we see that ΔC_p is 0.58 cal. per mole and $\Delta H_0°$ is -1540 cal. per mole. Therefore

$$\Delta H°=0.58T-1540. \qquad (2)$$

Integration of Eq. (1) gives us

$$\log K=0.292\log T+\frac{336.5}{T}+I. \qquad (3)$$

Substituting into Eq. (3) the experimental values for K with their corresponding temperatures, we obtain the values for "I" shown in Table IV. These values show no drift over the 300° temperature range. We now have the complete equation

$$\log K=0.292\log T+\frac{336.5}{T}-1.055. \qquad (4)$$

From the values of ΔC_p and "I" we obtain for the entropy

$$\Delta S°=1.34\log T-4.25. \qquad (5)$$

Combining this with our previous expression for $\Delta H°$ we have:

$$\Delta F°=-4.83T-1.34T\log T-1540. \qquad (6)$$

To test our equations we use them to calculate K and compare the value obtained, K_{calc}, with that of our experiments, K_{exp}, and with that, K_{theo}, calculated from pure theory by W. F. Libby. This comparison is contained in Table V. In each case our calculated value of K lies within the root mean square error of the

TABLE III.

log 'K	log K	$1/T'$	$1/T$	$1/T$ °K Av.	T °K	log 'K −log K	Slope
0.4356	0.3293	0.0021	0.0017	0.0019	526	0.1063	267
0.4630	0.3546	22	18	0.0020	500	0.1084	271
0.4910	0.3816	23	19	21	476	0.1094	276
0.5200	0.4088	24	0.0020	22	454	0.1112	278
0.5486	0.4356	25	21	23	435	0.1130	282
0.5764	0.4630	26	22	24	417	0.1134	284
0.6050	0.4910	27	23	25	400	0.1140	285
0.6344	0.5200	28	24	26	385	0.1144	286
0.6630	0.5486	29	25	27	370	0.1144	286
0.6928	0.5764	0.0030	26	28	357	0.1164	291
0.7224	0.6050	31	27	29	345	0.1174	293
0.7520	0.6344	32	28	0.0030	333	0.1176	294
0.7810	0.6630	33	29	31	323	0.1180	295
0.8105	0.6928	34	0.0030	32	313	0.1177	294

TABLE IV.

T° K	log K_{obs}	log T	$\frac{-0.292}{\log T}$	$-336.5/T$	I
289.1	0.8293	2.461	0.719	1.164	−1.054
293.3	0.8109	2.467	0.720	1.148	−1.057
298.1	0.7959	2.474	0.722	1.129	−1.055
329.3	0.7033	2.517	0.734	1.022	−1.053
352.7	0.6405	2.547	0.744	0.954	−1.057
384.3	0.5752	2.585	0.755	0.876	−1.056
431.5	0.4914	2.635	0.769	0.780	−1.058
490.2	0.4216	2.690	0.785	0.687	−1.050
576.0	0.3365	2.760	0.806	0.585	−1.054

Av. $I=-1.055\pm0.002$

experimental value, with no drift being shown in these slight deviations.

The relationship between the experimental constants and W. F. Libby's theoretical calculations is demonstrated in Fig. 4. In it the lower curve represents the theory and the upper curve these experiments. The radius of the circles represents, in the case of the experiments, the root mean square error of the point while the circles around the theoretical points are an estimate by W. F. Libby of their probable errors. It is interesting to note that in a direction perpendicular to the curves, the "smearing" produced by these errors just overlaps.

The small difference between the two curves corresponds at 16°C to a $\Delta F°$ difference of 24 cal. per mole out of about 1100 cal. This is much too high to be due to error in the fundamental frequencies of the water molecule. The discrepancy, therefore, must be due either to some unaccounted source of systematic error in the experiments or to some inadequacy in the assumptions used in the theoretical calculations. One of the possibilities in the latter case, and the initial interest behind W. F. Libby's calculations, is that the potential function for a molecule may, in fact, be changed by isotopic substitution.

TABLE V.

t °C	log K_{calc}	K_{calc}	K_{exp}	K_{theo}
16.0	0.828	6.73	6.75±0.04	6.47
20.2	0.813	6.50	6.47±0.12	6.24
25.0	0.796	6.25	6.25±0.05	6.01
56.2	0.701	5.02	5.05±0.05	4.84
79.6	0.643	4.40	4.37±0.05	4.23
111.2	0.576	3.77	3.76±0.04	3.64
158.4	0.494	3.12	3.10±0.06	3.03
217.1	0.417	2.61	2.64±0.04	2.54
302.9	0.336	2.17	2.17±0.02	2.08

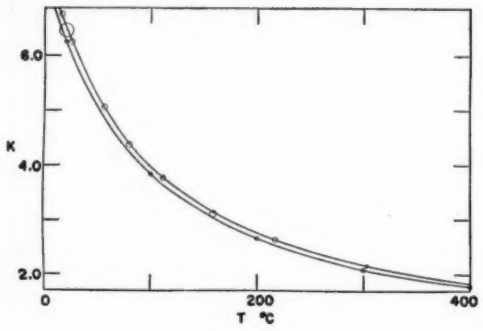

FIG. 4.

The agreement is actually so close, however, as to constitute quite a satisfactory check over the entire temperature range. It can be said with confidence that isotopic substitution by elements other than hydrogen will produce no effect upon the potential function of a molecule.

ACKNOWLEDGMENTS

We wish to thank Professor W. F. Libby of the University of California for his counsel and advice in the planning and manipulative details of these experiments and also the Radiation Laboratory of the University of California for the radioactive water employed.

THE JOURNAL OF CHEMICAL PHYSICS VOLUME 11, NUMBER 9 SEPTEMBER, 1943

The Use of the Exchange Between Carbon Dioxide, Carbonic Acid, Bicarbonate Ion, and Water for Isotopic Concentration*†

ALLEN F. REID AND HAROLD C. UREY
Department of Chemistry, Columbia University, New York, New York

(Received June 28, 1943)

A study was made of the exchange of oxygen and carbon in the reactions:

$$CO_2 \text{ (dissolved)} + H_2O \rightleftarrows H_2CO_3,$$
$$CO_2 \text{ (dissolved)} + OH^- \rightleftarrows HCO_3^-.$$

It was found that the rate of the first could be increased four or five times and the rate of the second up to 2000 times by heterogeneous catalysis. Investigation of the use of these catalyzed reactions for separation of the oxygen and carbon isotopes was carried out both by the use of a static bomb technique and by the operation of fractionating columns. The effects of different operating conditions were indicated, and the necessity for turbulent flow in the gas phase was established. Pressures from one through fifty atmospheres were tried, as the increase of CO_2 pressure increases the concentration of CO_2 (dissolved) and thus speeds up the exchange.

A comparison of the above method with the $HCN-CN^-$ method of separation of carbon isotopes shows the cyanide exchange to be somewhat faster and to require less time to come to production, somewhat doubtful advantages when they must be coupled with the polymerization and poisonous properties of the hydrogen cyanide, as well as with its greater cost.

INTRODUCTION

ONE comparatively new but, nevertheless, powerful tool in the study of carbon and oxygen is the use of isotopic tracers, which also show promise of value in certain types of quantitative analysis. Chemical methods of obtaining small quantities of material with different isotopic concentrations than normal have been used for some time.

The two-phase system, sodium cyanide solution—hydrogen cyanide gas was successfully used[1] to concentrate C^{13}, but possessed the disadvantages of polymerization of the hydrogen cyanide in the presence of sodium cyanide and of the highly poisonous character of hydrogen cyanide. The method used here was the operation of a packed fractionating column by passing hydrogen cyanide up the column countercurrent to the sodium cyanide solution, and supplying reflux at the top. Similar systems using carbon dioxide in exchange with bicarbonate ion in solution were tried with many types of homogeneous catalysts but without success,[2] as the exchange was very slow and not suitable for these counter-current methods. We decided that investigation of the possibilities of heterogeneous catalysis for that exchange might yield an exchange rate high enough to be suitable. The reactions between carbon dioxide and water result in a fractionation factor favorable for an isotopic concentration of both C^{13} and O^{18}, respectively:

$$C^{13}O_2 + xH_2C^{12}O_3 + (1-x)HC^{12}O_3^- = C^{12}O_2 + xH_2C^{13}O_3 + (1-x)HC^{13}O_3^-$$
$$CO_2{}^{16} + 2H_2O^{18} = CO_2{}^{18} + 2H_2O^{16}.$$

Since in the cyanide system and other similar systems the exchange was much faster than here, it follows that the reaction is not diffusion controlled, but that the slow process is in the exchange indicated by (1) and (2):

$$CO_2 \text{ (dissolved)} + OH^- \underset{k_{-1}}{\overset{k_1}{\rightleftarrows}} HCO_3^-, \qquad (1)$$

$$CO_2 \text{ (dissolved)} + H_2O \underset{k_{-2}}{\overset{k_2}{\rightleftarrows}} H_2CO_3 \qquad (2)$$

Faurholt[3] in 1924, Brinkman, Margaria, and Roughton[4] in 1933, Stadie and O'Brien[5] in 1935,

* Submitted in partial fulfillment of the requirements for the degree of Doctor of Philosophy, in the Faculty of Pure Science, Columbia University.

† Publication assisted by the Ernest Kempton Adams Fund for Physical Research of Columbia University.

[1] Hutchison, Stewart, and Urey, J. Chem. Phys. **8**, 523 (1940).

[2] G. A. Mills and H. C. Urey, J. Am. Chem. Soc. **62**, 1019 (1940).

[3] C. Faurholt, J. Chim. Phys. **21**, 400–455 (1924) (rate const. must be multiplied by 2.3).

[4] Brinkman, Margaria, and Roughton, Phil. Trans. Roy. Soc. **A232**, 65 (1933).

[5] W. C. Stadie and H. O'Brien, J. Biol. Chem. **103**, 521 (1933); **112**, 723 (1936).

Roughton and Booth[6] in 1938, and Mills and Urey[2] in 1940 have all determined rate constants for some of the above reactions by various methods. It is evident that the problem to be solved to make possible a practical method of using the above exchanges for isotopic concentration is to increase the rate of the slow process while keeping a conservatively low temperature, as the fractionation factor decreases with rise in temperature.[7]

Cohen[8] set up equations corresponding to the following for isotopic exchange in packed columns:

$$H\frac{\partial N}{\partial t}=L\frac{\partial N}{\partial z}-kcC\{N(1-n)-\alpha n(1-N)\}, \quad (3)$$

$$h\frac{\partial n}{\partial t}=-l\frac{\partial n}{\partial z}+kcC\{N(1-n)-\alpha n(1-N)\}, \quad (4)$$

where k is a constant; C is the concentration in moles per unit volume of carbon in the liquid; N is the mole fraction of heavy carbon in the liquid; H is the moles of holdup per unit length of combined light and heavy carbon in the liquid; L is the flow of light and heavy carbon in the liquid in moles per unit time; and where lower case symbols designate the corresponding quantities in the gas phase, z is the distance along the column measured from the reflux end, and at equilibrium:

$$\alpha=\frac{N(1-n)}{n(1-N)}. \quad (5)$$

Inspection of (4) and (5) indicates at once that for any given column the highest fractionation is obtained with the highest value of kcC. However, that factor is an exchange rate constant per unit length of column, and as such varies from column to column with the cross-sectional area, whereas we wish to find the exchange rate per unit volume of packing, irrespective of the size of the particular column used. That factor then turns out to be kcC/A, where A is the cross-sectional area, and is the quantity we wish to maximize.

Introducing the boundary condition that at $z=0$, $N=n$, and solving (4) and (5), we find that for total reflex and no production at $z=0$; that is, $l=L$,

$$\frac{kcCz}{L}=\frac{2}{\alpha-1}[\tanh^{-1}(1-2N_z)-\tanh^{-1}(1-2N_0)]. \quad (6)$$

If $L=l-P$, where P is the number of moles per unit time drawn off at the reflux end, then

$$LN-ln=PN_0, \quad \text{and if} \quad p\equiv P/L \quad (7)$$

$$\frac{kcCz}{L(1-p)}=\frac{2}{(B^2-4AD)^{\frac{1}{2}}}\left[\tanh^{-1}\frac{2AN_z+B}{(B^2-4AD)^{\frac{1}{2}}}-\tanh^{-1}\frac{2AN_0+B}{(B^2-4AD)^{\frac{1}{2}}}\right], \quad (8)$$

where

$$A\equiv\alpha-1,\ B\equiv1-p+pN_0-\alpha pN_0-\alpha,\ D\equiv\alpha pN_0.$$

In these equations, $kcCz/L$ corresponds to the number of theoretical plates in the column.

Corresponding equations are applicable to oxygen fractionation.

Another aspect to be considered is the time required for any given column to approach equilibrium, as it would be easy to fashion a system in which this would take a prohibitive time.

Cohen finds that when $l/h\gg L/H$ and $h+H\alpha\gg H(1-\alpha)$

$$T=\frac{H}{(1-\alpha)^2L\nu F(\sigma)}, \quad (9)$$

where ν is the number of plates/unit length, T being defined as the time required for the principal transient term in his expansion to diminish to $1/e$th of its initial value. $F(\sigma)$ is a function of the ratio of the abundance ratios at the two ends of the column, decreasing very rapidly with increase of that ratio.

In the case of high pressures in the system, (9) would not hold as well, but by multiplication by $(h+H)/H$, one would expect fair agreement, as the amount of concentrate to be stripped is greater by that factor than in the case where h is negligible.

[6] F. J. W. Roughton and V. H. Booth, Chem. and Ind. **56**, 1053 (1937).
[7] H. C. Urey and L. J. Greiff, J. Am. Chem. Soc. **57**, 321 (1935).
[8] K. Cohen, J. Chem. Phys. **8**, 588–597 (1940).

TABLE I.

Exp. no.	Time of reaction	$\left(\frac{CO^{18}O^{16}}{CO_2^{16}}\right)_{normal}/\frac{CO^{18}O^{16}}{CO_2^{16}}$ Sample	Equilibrium	$\tau_{\frac{1}{2}}$	Moles CO_2	Moles H_2O	Bomb volume in cc	kcC/A moles/cc min.
9	5 min.	1.11	1.27	5.62 min.	0.0060	0.0833	3.2	4.06×10^{-4}
9	15 min.	1.22	1.27	5.61 min.	.0060	.0833	3.2	4.05×10^{-4}
25	20 sec.	1.07	1.44	80 sec.	0.0031	0.0566	5.0	5.83×10^{-4}
25	30 sec.	1.09	1.44	90 sec.	.0031	.0556	5.0	5.18×10^{-4}

EXPERIMENTAL

Determination of α

In order to interpret the results of column experiments properly it is necessary to know the value of α. Urey and Greiff[7] in 1935 calculated the constant

$$\alpha' = \frac{[C^{12}O_2][C^{13}O_3^{=}]}{[C^{13}O_2][C^{12}O_3^{=}]}$$

at 25°C to be 1.012. This should be an approximation to the value of

$$\alpha = \frac{[C^{12}O_2][HC^{13}O_3^{-}]}{[C^{13}O_2][HC^{12}O_3^{-}]}.$$

Urey, Aten, and Keston[9] found an experimental value of about 1.013 or 1.014 for α using the equilibrium between $KHCO_3$ solution and CO_2. In an independent determination we bubbled normal CO_2 for 24 hours through 2 M NH_4HCO_3. Samples were taken and analyzed on a Nier type mass spectrometer until they checked to within 0.1 percent. A correction was made for the O^{17} abundance, and α was calculated.

Run	Sample	α
A	1	1.0070
A	2	1.0120
B	1	1.0159
B	2	1.0132
	Mean	1.0120 ± 0.0025

The fairly large spread of these values was due to spectrometer errors.

Throughout the calculations in this paper, the value of α used was 1.012.

Static Experiments

Due to the inconvenience and large time consumption necessary to set up and operate a fractionation column to investigate each type of packing under each set of experimental conditions, as well as because of the large amount of packing necessary for such experiments, we decided to investigate first the rates in small reaction vessels. Such a vessel would be filled with the packing, moistened with the liquid phase, filled with the gas phase and allowed to stand for a limited length of time. Then analysis of the resulting contents would indicate the rate of reaction. In such a system,

$$l=L=0 \quad \text{and} \quad hn+HN=hn_\infty+HN_\infty.$$

If n is small, (4) and (5) yield:

$$\frac{kcC}{A} = \frac{0.693\frac{h}{A}\times\frac{H}{A}}{\tau_{\frac{1}{2}}\left(\frac{h+\alpha H}{A}\right)}, \tag{10}$$

where $\tau_{\frac{1}{2}}$ is the time required for the system to come half-way to equilibrium, and h/A and H/A measure the holdup per unit volume in the gas and liquid phases, respectively.

Copper and steel bombs were loaded with packing to be investigated for possible catalytic effect. In most cases about 20 percent of the total bomb space was filled with water or bicarbonate solution with a lower than normal O^{18} content. This was enough totally to wet the packing without apparent surplus. In some cases an aqueous solution of bicarbonate with a greater than normal C^{13} content was used. In these cases a larger proportion of solution, up to 50 percent of the total space, was used so that there would be sufficient excess C^{13} to give a measurable enrichment of the added CO_2. Then the packing was at about the limit of liquid holdup without flooding. In the latter case the expected exchange

[9] Urey, Aten, and Keston, J. Chem. Phys. **4**, 622 (1936).

TABLE II.

Exp. no.	Packing	Solution	Temp. °C	Pressure CO_2 lb./in.²	$kcC/A \times 10^5$ moles/cc min. O-exchange	C-exchange
1	$BaCO_3$	H_2O, 0.111% H_2O^{18}	23	265	2.77	
2	20% $BaCO_3$ on Al_2O_3	H_2O, 0.111% H_2O^{18}	23	265	4.04	
3	20% $BaCO_3$ on Al_2O_3	H_2O, 0.111% H_2O^{18}	23	765	14.8	
4	Diatomaceous earth	H_2O, 0.111% H_2O^{18}	26	765	14.1	
5	Silica gel	H_2O, 0.111% H_2O^{18}	24	765	35.0	
6	Calcined silica gel	H_2O, 0.111% H_2O^{18}	25	765	59	
7	20% $PbCO_3$ on Al_2O_3	H_2O, 0.111% H_2O^{18}	23	85	7.5	
8	20% $PbCO_3$ on Al_2O_3	H_2O, 0.111% H_2O^{18}	23	265	18.2	
9	20% $PbCO_3$ on Al_2O_3	H_2O, 0.111% H_2O^{18}	23	765	40.	
10	20% $PbCO_3$ on Al_2O_3	H_2O, 0.111% H_2O^{18}	0	765	0–2	
11	20% $PbCO_3$ on Al_2O_3	H_2O, 0.111% H_2O^{18}	64	765	80	
12	Al_2O_3, 15.2% H_2O	H_2O, 0.111% H_2O^{18}	24	265	38	
13	Al_2O_3, 15.2% H_2O	H_2O, 0.111% H_2O^{18}	28	765	140	
14	Al_2O_3, 15.2% H_2O	2.1 M $KHCO_3$, 4.7% $KHC^{13}O_3$	29	765		260
15	Morell Char. no. 7	H_2O, 0.111% H_2O^{18}	13.2	765	127	
16	Morell Char. no. 7	H_2O, 0.111% H_2O^{18}	23.5	765	351	
17	Morell Char. no. 7	H_2O, 0.111% H_2O^{18}	48	765	351	
18	Morell Char. no. 7*	H_2O, 0.111% H_2O^{18}	25	765	77	
19	Morell Char. no. 7	2.1 M $KHCO_3$, 4.7% $KHC^{13}O_3$	25	765		210
20	Morell Char. no. 7	2.1 M $KHCO_3$, 4.7% $KHC^{13}O_3$	25	265		110
21	Morell Char. no. 7	2.1 M $KHCO_3$, 3.1% $KHC^{13}O_3$	23.4	72		30
22	Fiber A: Corning Fiber Glass no. 9930	2.1 M $KHCO_3$, 4.7% $KHC^{13}O_3$	27	55		262
23	Fiber A: Corning Fiber Glass no. 9930	2.1 M $KHCO_3$, 4.7% $KHC^{13}O_3$	27	265		450
24	Fiber A: Corning Fiber Glass no. 9930	2.1 M $KHCO_3$, 4.7% $KHC^{13}O_3$	26	765		630
25	Fiber B: Corning Fiber Glass no. 790	H_2O, 0.111% H_2O^{18}	23	265	55.0	
26	Fiber B: Corning Fiber Glass no. 790	0.50 M $KHCO_3$, 0.113%[H_2O^{18}+$KHCO_2O^{18}$]	24	265	123	
27	Fiber B: Corning Fiber Glass no. 790	2.1 M $KHCO_3$, 0.119%[H_2O^{18}+$KHCO_2O^{18}$]	24	265	280	

* After ageing 41 days.

TABLE III.* Calculation of constants from $kcC/A = (k_1[OH^-]+k_2[H_2O])[CO_2]/W$.

Exp no.	Packing	kcC/A (moles·liter^{-1}·min.$^{-1}$)	$[CO_2]$	$[OH^-]$	W	$k_1[OH^-]+k_2[H_2O]$ (min.$^{-1}$)	k_1 (mole^{-1}·min.$^{-1}$)	$k_2[H_2O]$ (min.$^{-1}$)
22	Fiber A	2.62	0.152	1.31×10^{-7}	2.0	34.8		
							2.08×10^8	6.0
23	Fiber A	4.50	0.63	3.92×10^{-8}	2.0	14.3		
							2.02×10^8	6.4
24	Fiber A	6.30	1.18	2.14×10^{-8}	2.0	10.7		
							2.05×10^8	6.2
Average	Fiber A							
25	Fiber B	0.55	0.63	1.5×10^{-11}	5.0	4.4		
							3.6×10^8	4.4
26	Fiber B	1.23	0.63	1.5×10^{-8}	5.0	9.8		
							5.1×10^8	2.2
27	Fiber B	2.80	0.63	3.92×10^{-8}	5.0	22.2		
							4.3×10^8	3.3
Average	Fiber B							

* All experiments are at room temperature.

rate would be smaller than in the former, due to a smaller catalytic area per unit volume of solution.

After loading the bombs, the air was pumped out and normal CO_2 was let in at the proper pressure. Samples of the gas were drawn out at

appropriate intervals (generally from $\frac{1}{2}$ to 2 half-conversion periods) and analyzed on a Nier type mass spectrometer. The constant kcC/A was then calculated from (10). Table I shows some sample data used in the calculations. The equilibrium value of

$$\left(\frac{CO^{18}O^{16}}{CO_2^{16}}\right)_{\text{normal}} \Big/ \frac{CO^{18}O^{16}}{CO_2^{16}}$$

was found by leaving the CO_2 in contact with the solution for a long time. Table II gives a summary of the results. The precision was limited mainly by the spectrometer analyses, but was generally within 1'5 percent.

The interpretation of kcC/A in terms of the rate constants in reactions (1) and (2) is made by following each isotope separately. For carbon exchange:

$$C^{12}O_2+OH^- \underset{k_{-1}}{\overset{k_1}{\rightleftarrows}} HC^{12}O_3^-, \qquad (1)$$

$$C^{13}O_2+OH^- \underset{k_{-1}'}{\overset{k_1'}{\rightleftarrows}} HC^{13}O_3^-, \qquad (1')$$

$$C^{12}O_2+H_2O \underset{k_{-2}}{\overset{k_2}{\rightleftarrows}} H_2C^{12}O_3, \qquad (2)$$

$$C^{13}O_2+H_2O \underset{k_{-2}'}{\overset{k_2'}{\rightleftarrows}} H_2C^{13}O_3, \qquad (2')$$

$$\alpha_1=\frac{k_1'k_{-1}}{k_1k_{-1}'}; \quad \alpha_2=\frac{k_2'k_{-2}}{k_2k_{-2}'}. \qquad (11)$$

Considering only (1) and (1'):

$$\frac{d[HC^{12}O_3^-]}{dt}=k_1[C^{12}O_2][OH^-] - k_{-1}[HC^{12}O_3^-], \qquad (12)$$

$$\frac{d[HC^{13}O_3^-]}{dt}=k_1'[C^{13}O_2][OH^-] - k_{-1}'[HC^{13}O_3^-]. \qquad (12')$$

If W is the volume ratio of the reaction vessel to the solution,

$$\frac{H_1}{A}=\frac{[HCO_3^-]}{W}. \qquad (13)$$

Assuming

$$N=\frac{[HC^{13}O_3^-]}{[HCO_3^-]}=\frac{[H_2C^{13}O_3]}{[H_2CO_3]},$$

and with

$$n=\frac{[C^{13}O_2]}{[CO_2]}$$

$$\frac{dN}{dt}=\frac{d[HC^{13}O_3^-]-Nd[HCO_3^-]}{[HCO_3^-]dt}. \qquad (14)$$

From (11), (12), (13), and (14):

$$\frac{H}{A}\frac{dN}{dt}=\frac{1}{W}[OH^-][CO_2]\left\{\alpha n(1-N)\frac{k_{-1}'}{k_{-1}}k_1 - N(1-n)\left[k_1+\frac{(1-N)}{(1-n)}\left(1-\frac{k_{-1}}{k_{-1}'}\right)\times\frac{k_{-1}[HCO_3^-]}{[OH^-][CO_2]}\right]\right\}, \qquad (15)$$

which is in nearly the same form as Cohen's

TABLE IV. Rate constants for exchange reactions.

Observer	Temp. °C	k_1·mole·min.	k_{-1}·min.	$k_2[H_2O]$·min.	k_{-2}·min.
Faurholt (ref. 3)	0	(5.58×10⁴)	(3.54×10⁻⁴)	(0.180)	(137)
	18	(24.0×10⁴)	(41.6×10⁻⁴)	(1.52)	(980)
	25	[42.0×10⁴]	[110.0×10⁻⁴]	[3.50]	[2120]
Brinkman *et al.* (ref. 4)	0	(5.05×10⁴)		(0.156)	(102)
	18	(12.3×10⁴)		(1.44)	(666)
	25	[17.5×10⁴]		[3.46]	[1400]
Mills and Urey (ref. 2)	0			(0.162)	
	0			0.123	
	25			1.65	
This paper	25				
	with Fiber *A*	(2.0×10⁸)	(4.4)	(6.2)	(5500)
	with Fiber *B*	(4.3×10⁸)	(9.5)	(3.3)	(2900)

All values in parentheses ( ) are measured in buffered solutions.
Values in brackets [ ] are extrapolated.

TABLE V.*

Exp. no.	Packing	Pressure atmos.	Base used	Diameter of column (in.)	Height of column (ft.)	Flow moles/cm² min.	$\frac{r(z)}{r(0)}$ analysis	$\frac{r(z)}{r(0)}$ extr. to $t=\infty$	$kcCz/L$	kcC/A moles/cm² min.
1	Morell Char. no. 7	5	2.3 *M* KOH	0.6	10	1.02×10^{-3}	1.10	1.10	8.0	2.7×10^{-5}
2	Morell Char. no. 7	54	2.3 *M* KOH	0.6	10	1.29×10^{-3}	1.038	1.038	3.1	1.34×10^{-5}
3	⅛″ Pyrex helices	1	1.3 *M* NH_4OH	0.6	12	1.38	1.003	1.003		0.096×10^{-5}
4	⅛″ Pyrex helices	1.3	2.3 *M* KOH	0.6	10	0.78	1.11	1.11	8.8	2.3×10^{-5}
5	etched 5	4	2.3 *M* KOH	0.6	10	0.78	1.14	1.14	11	2.8×10^{-5}
6	min.**	50	20% ethandomine	0.6	10	0.98	1.064	1.064	5.2	1.7×10^{-5}
7	⅛″ Pyrex helices	1	1.8 *M* NH_4OH	0.6	11.8	1.06	1.093	1.103	8.2	2.4×10^{-5}
8	etched 23 min.	1	2.0 *M* NH_4OH	0.6	12	4.00	1.028	1.035	2.9	3.2×10^{-5}
9	⅛″ Pyrex helices etched 23 min.	1	5.1 *M* NH_4OH	0.6	11.8	4.00	1.032	1.035	2.9	3.2×10^{-5}
10	⅛″ Pyrex helices etched 23 min.	18	2.6 *M* NH_4OH	0.6	12	8.50	1.020	1.027	2.2	5.1×10^{-5}
11	⅛″ Pyrex helices etched 23 min.	18	2.6 *M* NH_4OH	0.6	12	17.3	1.044	1.100	8.0	38×10^{-5}
12	⅛″ Pyrex helices etched 23 min.	50	2.5 *M* NH_4OH	0.6	12	16.4	1.083	1.1100	8.8	40×10^{-1}
13	⅛″ Pyrex helices etched 23 min.	50	2.5 *M* NH_4OH	0.4	3	34.2	1.012	1.013	1.1	40×10^{-5}
14	6–8 mesh Haydite	16	2.4 *M* NH_4OH	0.6	12	15.9	1.032	1.032	2.64	11.5×10^{-5}
15	Haydite 6–8 mesh	16	2.4 *M* NH_4OH†	0.6	12	15.9	1.032	1.032	2.64	11.5×10^{-5}
16	Etched 6–8 mesh Haydite	16	2.3 *M* NH_4OH	0.6	12	16.1	1.074	1.100	8.0	35.4×10^{-5}
17	Etched 6–8 mesh Haydite	6	2.3 *M* NH_4OH	0.6	12	15.4	1.030	1.030	2.5	10.5×10^{-5}
18	Etched 6–8 mesh Haydite	33	2.4 *M* NH_4OH	0.6	12	15.5	1.093	1.100	8.0	33.8×10^{-5}
19	Etched 6–8 mesh Haydite	16	2.3 *M* NH_4OH	0.6	12	7.0	1.055	1.055	4.5	8.7×10^{-5}

* All runs are at room temperature.
** All etching done with 8.4 per cent HF solution.
† Agitated with etchings.

equation. When k_{-1} and n and N are small:

$$\frac{H_1}{A}\frac{\partial N}{\partial t}=\frac{k_1}{W}[OH^-][CO_2](\alpha_1 n-N). \quad (16)$$

A similar equation holds for Eqs. (2) and (2′):

$$\frac{H_2}{A}\frac{\partial N}{\partial t}=\frac{k_2}{W}[H_2O][CO_2](\alpha_2 n-N). \quad (17)$$

Assuming that α_1 and α_2 are near enough to the same value so that we may use a common value α, then

$$\frac{H}{A}\frac{\partial N}{dt}=(k_1[OH^-]+k_2[H_2O])\frac{[CO_2]}{W}(\alpha n-N). \quad (18)$$

A similar equation holds for oxygen exchange. We can now equate kcC/A to

$$(k_1[OH^-]+k_2[H_{20}])\frac{[CO_2]}{W}.$$

Then, with our values of kcC/A we can determine the rate constants k_1 and $k_2[H_2O]$ if we have at least two different sets of conditions for a single packing. The calculations of those constants are shown for the two Pyrex fibers in Table III, and a comparison with other values is shown in Table IV. The catalysis of reaction (1) is quite large.

In the above calculations the *p*H of the water solution was taken from Moore's tables.[10] The solubility of CO_2 was taken from Sander's values.[11] The constants used were:

$$-\log K_{a\,25°}=6.345-0.119\omega, \quad (19)[12]$$

where ω is the ionic strength. Thus, with $\omega=0$,

$$K_{a\,25°}\equiv\frac{[H^+][HCO_3^-]}{[H_2CO_3]+[CO_2\,(\text{dissolved})]}=4.52\times10^{-7}$$

[10] M. B. Moore, with J. H. Buchanan, Iowa State College J. Sci. **4**, 431–40 (1930).
[11] W. Sander, Zeits. f. physik. Chemie **78**, 513–49 (1912).
[12] D. A. MacInnes, *Principles of Electrochemistry* (Reinhold, 1939).

and

$$\frac{[CO_2\ (\text{dissolved})]}{[H_2CO_3]} = 880. \qquad (20)^{13-16}$$

Column Experiments

The results from the reaction vessel experiments showed enough promise so that actual fractionation in packed columns was tried. The choice of the packing was indicated by the static experiments. Activated charcoal was tried; then Pyrex helices. Next, the helices were etched so as more closely to simulate the Pyrex fiber surface. Then a cheap, siliceous, shale packing, Haydite, was tried, both unetched and etched. A control using the unetched Haydite and a solution agitated with etchings was run to make sure that the increased rates were not due to homogeneous catalysis from some material left on the etched surface. The runs were made at room temperature. Pressures from one to fifty atmospheres were tried. The procedure was straightforward: Columns were filled with the packing to be investigated. The column was filled with CO_2 and a solution of base was introduced at the top at the rate desired, reacting with the CO_2 to form HCO_3^-, which traveled down the column. Normal CO_2 was fed in at the bottom at constant pressure. In these experiments, since the heavier carbon concentrates in the liquid phase, the C^{12} concentrated at the top. A steady drain took place at the bottom while samples of the gas were drawn off at the top and analyzed. kcC/A was then calculated from (7). A summary is given in Table V, illustrated in part by Figs. 1, 2, and 3.

In most instances the equilibrium value of $r(z)/r(0)$, where r is the ratio of the heavy to the light isotope, was determined by analyzing one sample near the first part of the run and getting checks on the same value from two successive samples after equilibrium should have been reached.

Experiment No. 4, a little more detailed, is outlined in Fig. 4. The measured holdup of solution was 50 cc. From the data given and (9), $T=4.4$ hours; whereas, from the experimental curve, $T=5.2$ hours, in fair agreement with Cohen's theory.

Fluid flow theory states that in flow through a packed column, a fluid maintains laminar flow only up to a given critical value of the Reynolds number. When μ is the viscosity coefficient, ρ is the density, U is the linear velocity, and d is a measure of the spacing between the packing, the Reynolds number is given by

$$R_e = dU\rho/\mu.$$

The critical value is around 40, depending on the type of packing; however, it is rather loosely determined for any particular application. In the

[13] E. R. Strohecker, Zeits. f. Nahr.-Genussm. **31**, 121–60 (1926).
[14] O. Haehnel, Centr. Mineral Geol. **1920**, 25–32 (1920).
[15] F. J. J. Buytendyke, R. Brinkman, and H. W. Mook, Biochem. J. **21**, 576–84 (1927).
[16] E. Müller and A. Luber, Zeits. f. anorg. allgem. Chemie **190**, 427 (1930).

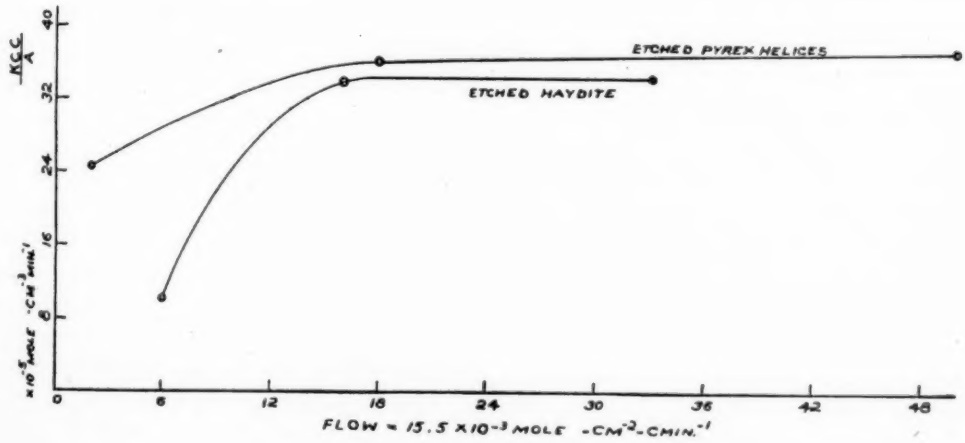

FIG. 1.

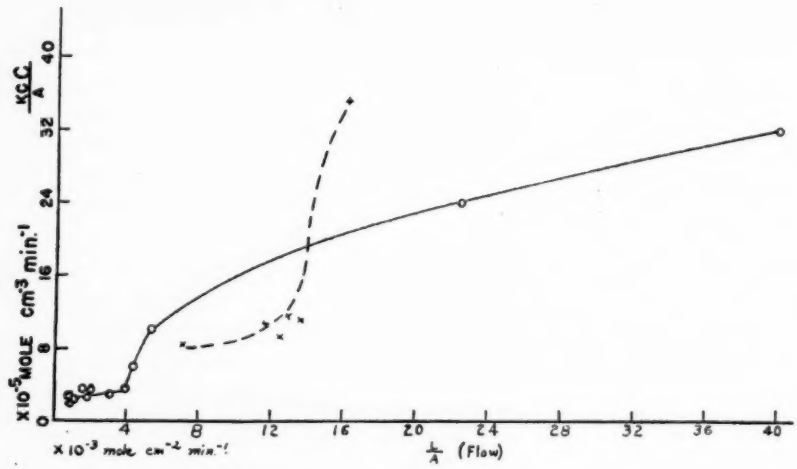

FIG. 2. Pyrex helices, etched 23 min., 1 atmos. —o—.
6–8 mesh Haydite, etched 23 min., 16 atmos. ---×---.

four cases most widely investigated, shown in Figs. 3 and 4, the approximate gas flow rate to Reynolds number correspondence was determined. Using a value of 0.7 cm for d, $R_e = 3 \times 10^3\ U$ min. cm²/mole. This would place the large increase of kcC/A per unit flow at a Reynolds number from 25 to 50 for all the cases except the atmospheric run. From this it seems likely that the establishment of turbulence is responsible for the increase, and since much slower rates of flow have produced faster exchange in other systems, it appears that diffusion through the liquid to the catalytic surface is rate controlling, and may be speeded up by producing turbulence in the gas.

From the results obtained, the specifications of an efficient system for fractionating carbon or oxygen isotopes by the above method should include:

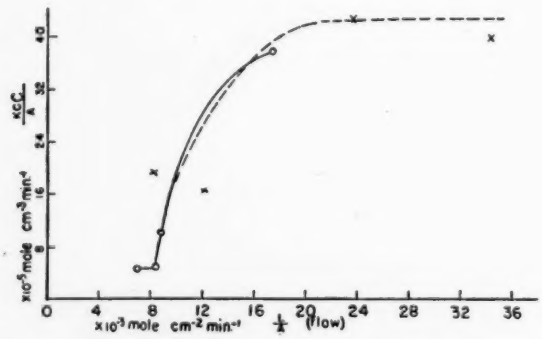

FIG. 3. Pyrex helices, etched 23 min., 18 atmos. —o—.
Pyrex helices, etched 23 min., 50 atmos. ---×---.

I. A pressure somewhat above 6 atmospheres up to 18 atmospheres so that [CO_2 (dis.)] is great enough.
II. A high enough pH so that advantage may be taken of catalyzed (1).
III. An economical packing (such as etched Haydite) with efficient fractionating characteristics and sufficient catalytic activity so that (1) and (2) are not rate controlling.
IV. A gas flow of sufficient velocity for turbulence.
V. As high a temperature as is necessary to keep the rate of (3) at the required value, but not too high, as α decreases with increasing temperature.[7]

Extension of Theory and Results to Large Scale Operation

Using the above results we calculated the specifications for erection and operation of a column system which would produce about 4 grams of carbon, 33 percent C^{13}, per day. In order to concentrate C^{13} to where it is about 50 percent of the C^{12} concentration, with $\alpha = 1.012$ and assuming normal CO_2 to be 1.10 percent C^{13}, 320 plates would be necessary. Because of the time required for a large single-stage system to come to equilibrium, usually a cascade system is designed for such high concentration.

This calculation is on such a six-stage cascade with the fractionation split evenly between the stages. The design is such that each unit has the

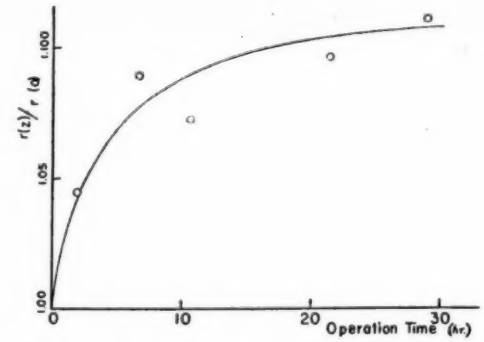

FIG. 4. Column experiment No. 4. 0.78 mole/cm² min. flow.

same C^{13} transport with a material flow such that 80 percent of the maximum C^{13} possible is stripped. The height of each column is calculated by (8).

The calculation of the time required for the cascade to come to production cannot be made by Cohen's theory, so another fairly accurate approximation was made. This consisted of determining the amount C^{13} over the normal there was in the cascade and dividing it by the rate at which C^{13} was stripped in the first column. If Q is the total moles of C^{13} in a column approximately

$$Q=(h+H)\int_0^z N_z dz. \tag{21}$$

With

$$r\equiv\left(\frac{N}{1-N}\right) \quad \text{and} \quad \nu\equiv\left(\frac{r_z}{r_0}\right)^{1/z},$$

assuming $r_z=r_0\nu^z$, (21) becomes

$$\begin{aligned} Q&=(h+H)\int_0^z \frac{r_0 V^z}{1+r_0 V^z}dz \\ &=\frac{h+H}{\ln V}\ln\left(\frac{1+r_z}{1+r_0}\right). \end{aligned} \tag{22}$$

If R is the number of moles of C^{13} stripped off in the first column A, then

$$R=L_A\int_0^T (N_{zA}-n_{zA})dt, \tag{23}$$

where T is the time required for equilibrium. If

$$\beta\equiv\frac{N_{zA}(1-n_{zA})}{n_{zA}(1-N_{zA})}$$

TABLE VI. Specifications for a 6-stage cascade. 16 atmospheres CO_2 with etched Haydite packing.

Unit	Inside diam. (inches)	Height (feet)	Flow of CO_2 moles/min.	% C^{13} at bottom
A	3.00	78	0.726	2.05
B	2.21	82	0.395	3.80
C	1.64	85	0.218	6.93
D	1.23	87	0.123	12.3
E	0.95	89	0.073	20.9
F	0.77	91	0.048	33.0

TABLE VII.

	Cyanide Cascade	Bicarbonate Cascade
kcC/A (operating)	1.012 8.1×10^{-4} moles cm^{-3} min.$^{-1}$*	1.012 3.5×10^{-4} moles cm^{-3} min.$^{-1}$
Size of 1st unit	40′×1″ diam.	78′×3″ diam.
Size of 2nd unit	25′×⅜″ diam.	82′×2.21″ diam.
Size of 3rd unit		85′×1.64″ diam.
Size of 4th unit		87′×1.23″ diam.
Size of 5th unit		89′×0.95″ diam.
Size of 6th unit		91′×0.77″ diam.
Flow through 1st unit	0.042 mole min.$^{-1}$	0.726 mole min.$^{-1}$
Production of C^{13}	0.161 g per day	1.46 g/day
$\frac{C^{13}}{C^{12}+C^{13}}$	0.23	0.33
Time to reach production	12 days	87 days

* Value for the 1″ column. For the ¾″ column, $kcC/A=2.8\times10^{-3}$ mole cm^{-3} min.$^{-1}$.

and N_{zA} is small

$$R=L_A N_{zA}\int_0^T \frac{\beta-1}{\beta}dt, \tag{24}$$

and assuming a mean value for β:

$$R=L_A N_{zA}\frac{(\beta-1)}{\beta}T. \tag{25}$$

We have for the complete system:

$$\Sigma Q_i=R+N_{zA}\Sigma(h_i+H_i)Z_i, \tag{26}$$

which becomes

$$T=\frac{\beta}{(\beta-1)L_A}\Sigma z_i(h_i+H_i)\times\left[\frac{\ln\left(\frac{1-N_{0i}}{1-N_{zi}}\right)}{N_{zA}\ln\frac{N_{zi}(1-N_{0i})}{N_{0i}(1-N_{zi})}}-1\right]. \tag{27}$$

In the above system using 6–8 mesh Haydite in the larger columns and 16 atmosphere of CO_2 (cf. Table VI)

$$H/A = 0.84 \times 10^{-3} \text{ mole/cm}^3,$$
$$h/A = 0.42 \times 10^{-3} \text{ mole/cm}^3.$$

The flow planned was 0.0160 mole/cm² min. Under these conditions a value of 3.5×10^{-4} mole/cm³ min. was used for kcC/A.

With $p_A = 0.000328$, the daily production is 1.46 g of C^{13}. The time to come to production, from (27), assuming $\beta = 1.011$, is 87 days.

Comparison of Cyanide and Bicarbonate Methods

A comparison of the $HCN - CN^{-}$[19] and $CO_2 - HCO_3^-$ methods of C^{13} concentration can be made by a glance at Table VII. For large scale operation, the cyanide method has the advantage of a smaller holdup and thus a shorter length of time to reach production. On the other hand, the raw materials are more expensive, and it has the aforementioned undesirable properties of polymerization and toxicity. In either case, the time necessary to reach production could be reduced by using a larger number of units in the cascade.

THE JOURNAL OF CHEMICAL PHYSICS VOLUME 11, NUMBER 9 SEPTEMBER, 1943

The Photographic Latent Image

I. Lattice Energy and Related Quantities for a Hypothetical Silver Bromide Crystal Having the Cubic ZnS Type of Structure*†

MAURICE L. HUGGINS
Eastman Kodak Company, Rochester, New York

(Received April 2, 1941)

The usual NaCl type of structure (*B1*) for silver bromide is compared with a hypothetical structure for this substance of the cubic ZnS type (*B3*) with regard to certain quantities which are of importance in connection with the theory of the photographic latent image. These include: lattice energy, equilibrium distance between closest atoms, density, potential at interstitial positions, potential energy changes as an ion moves from its normal position to an interstitial position, and as an ion or electron moves from one interstitial position to another. The methods of calculation are outlined and the probable accuracy of the results discussed.

INTRODUCTION

THE second paper of this series will contain a critical discussion of the hypothesis that, in the photographic latent image in a silver bromide crystal, the region immediately surrounding the photoelectrons has a structure of the *B3* (cubic ZnS) type—or another structure closely related to it—instead of the *B1* (NaCl) type structure possessed by the rest of the crystal (see Fig. 1).

Preliminary to this discussion it seems advisable to outline the methods and present the results of certain pertinent calculations, e.g., calculations of the approximate energy and dimensional changes to be expected from the *B1* to *B3* transformation and of the energy changes to be expected during the passage of Ag^+ ions, Br^- ions, or electrons through each of these types of structure.

LATTICE ENERGY OF AgBr HAVING THE *B1* TYPE STRUCTURE

Mayer[1] has computed a theoretical value of $13.5 \cdot 10^{-12}$ erg per molecule or 197 kcal. per mole

---

* Presented before the Division of Physical and Inorganic Chemistry at the St. Louis Meeting of the American Chemical Society, April 9, 1941.

† Communication No. 802 from the Kodak Research Laboratories.

[1] J. E. Mayer, J. Chem. Phys. **1**, 327 (1933).

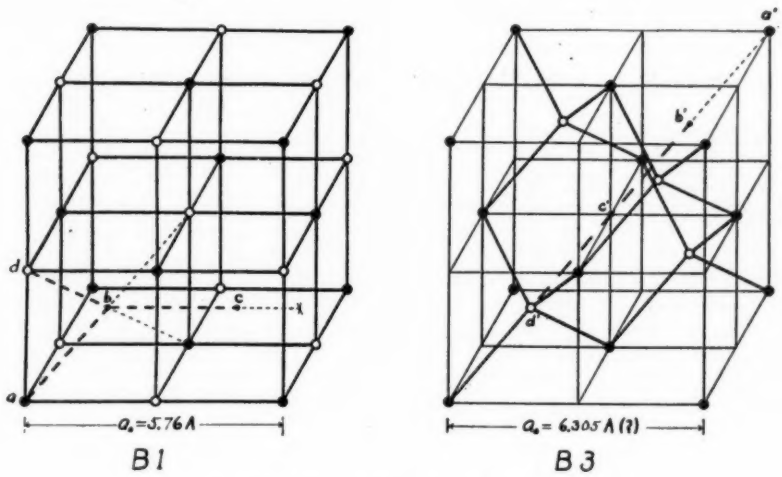

FIG. 1. Unit cubes of the *B1* and *B3* structures.

for the lattice energy, to be compared with an "experimental" value, computed by means of a "Born cycle," of 202 kcal. per mole. He suggests that the difference is primarily the result of the neglect in the theoretical calculation of any homopolar bond energy contribution.

In Mayer's treatment, certain constants in the exponential expression for the "overlap" repulsion energy between two ions were derived from Richards and Jones'[2] compressibility data for silver halide crystals. In view of Bridgman's[3] more recent results on these crystals, it seems that the probable accuracy of the data hardly warrants this procedure, rather than the simpler alternative of assuming the constant a, in the expression

$$\exp\left[a(r_{Ag}+r_{Br}-r)\right],$$

to be the same as that ($3.00\cdot10^8$ cm^{-1}) found to be satisfactory for all the alkali halides. This latter procedure, moreover, has the advantage of giving a value of r_{Ag} which is directly comparable with the other basic radii previously obtained.[4,5]

A recalculation of the lattice energy of silver bromide (*B1* type) has, therefore, been made, following strictly the procedure used[5] for the alkali halides and adopting Mayer's estimates of the van der Waals attraction constants. The value obtained is $13.2\cdot10^{-12}$ erg per "molecule." The difference between this and Mayer's value is certainly within the probable error of the calculation.

The value of r_{Ag} deduced in this calculation is $1.05\cdot10^{-8}$ cm. Using the approximate equation previously given [Eq. (5) of reference 5], with appropriate values of the constants, the compressibility is computed to be $2.4\cdot10^{-12}$ barye^{-1}. This is in sufficiently good agreement with Richards and Jones' value of $2.74\cdot10^{-12}$ and Bridgman's value (which, he states, is probably too low) of $2.30\cdot10^{-12}$.

NON-COULOMB INTERACTION ENERGIES

If the same constants are used as in the lattice energy calculations, the non-Coulomb interaction energy between two Ag^+ ions varies with the distance r between them according to the equation

$$\phi_{AgAg}=-67\cdot10^{-60}r^{-6}-91\cdot10^{-76}r^{-8}+1.111\exp\left[3(2.10-10^8r)\right]. \quad (1)$$

Similarly,

$$\phi_{AgBr}=-109\cdot10^{-60}r^{-6}-199\cdot10^{-76}r^{-8}+0.9305\exp\left[3(2.61-10^8r)\right] \quad (2)$$

and

$$\phi_{BrBr}=-208\cdot10^{-60}r^{-6}-475\cdot10^{-76}r^{-8}+0.750\exp\left[3(3.12-10^8r)\right]. \quad (3)$$

[2] T. W. Richards and G. Jones, J. Am. Chem. Soc. **31**, 158 (1909).
[3] P. W. Bridgman, Proc. Am. Acad. **74**, 21 (1940).
[4] M. L. Huggins and J. E. Mayer, J. Chem. Phys. **1**, 643 (1933).
[5] M. L. Huggins, J. Chem. Phys. **5**, 143 (1937).

Curves representing these three equations are shown in Fig. 2. Within the error of the calculation, ϕ_{AgAg} is zero for all interionic distances greater than 2.5A.

It should be noted that these equations and curves make no allowance for the polarization of each ion by the charge on the other. This polarization would increase the repulsion between two like-charged ions and increase the attraction (decrease ϕ) between two oppositely charged ions. For structures in which each positive ion is symmetrically surrounded by negative ions and vice versa, this polarization can probably be neglected.

LATTICE ENERGY AND INTERATOMIC DISTANCES FOR AgBr HAVING THE *B3* TYPE STRUCTURE

Silver iodide at room temperature exists in two closely related types of structure, designated[6] as *B3* and *B4*, of nearly equal stability; in both types, each ion is tetrahedrally surrounded by four of the other kind. It is of interest, for our present purpose, to compute the lattice energy of a hypothetical silver bromide crystal having the *B3* structure, for comparison with the lattice energy given above for the *B1* type.

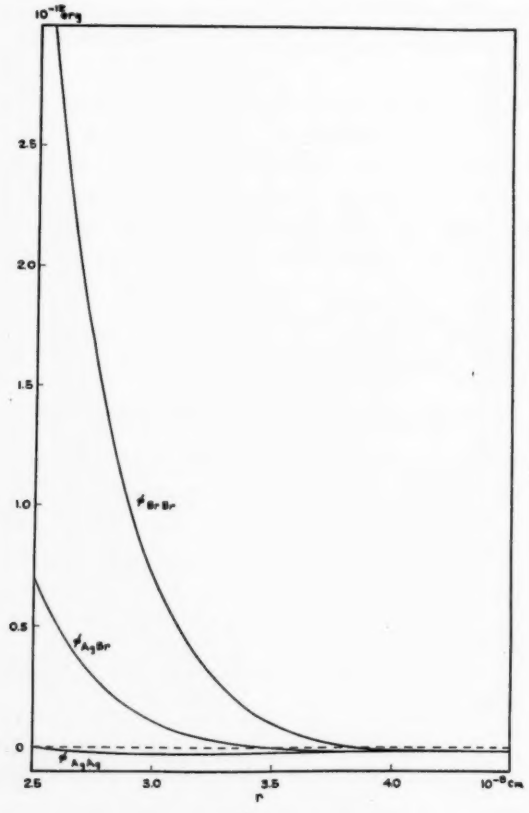

FIG. 2. Non-Coulomb interaction energies between pairs of ions, neglecting polarization.

The lattice energy depends on the scale of the structure, hence on the equilibrium distance between closest atoms. This distance can be computed, approximately, by the method of Huggins and Mayer [reference 4, Eq. (13)], using the same constants for the interactions between pairs of ions as in the calculations for the *B1* type. The assumption is involved that the structure can be treated as if purely ionic. This is doubtless a poorer assumption than for the *B1* type and some error is introduced on that account. The true equilibrium distance should be less than that computed.

The ratio of the thermal expansion coefficient to the compressibility also enters into the calculation, but large differences in the assumed ratio do not greatly affect the results. If one takes this ratio to be the same as for the *B1* type (expansion coefficient from *International Critical Tables*, compressibility from Richards and Jones[2]), the computed value of r_0 (the equilibrium distance between closest ionic centers) is 2.73A (and so $a_0 = 6.305$A).

The corresponding molecular volume and density are 62.7A^3 and 4.98 g/cc, respectively. These are 13 percent greater and less, respectively, than the corresponding quantities for the *B1* type. The computed value of the lattice energy for the *B3* structure is $12.79 \cdot 10^{-12}$. Comparison with the calculated lattice energy for the *B1* structure shows a difference in stability of about $0.4 \cdot 10^{-12}$ erg per molecule, i.e., about 0.3 electron-volt per molecule or 6 kcal. per mole. Since the *B3* structure (but not *B1*) is such that each atom can be bonded at the same time by (partially polar) covalent bonds to each of its close neighbors, one would expect the neglected contribution of the covalent bond energy to make the lattice energies—and so the stabilities—of the two types even more nearly equal.

[6] P. P. Ewald and C. Hermann, *Strukturbericht, 1913–1928* (Akademische Verlagsgesellschaft, Leipzig, 1931).

POTENTIAL ENERGY CHANGES FOR MOTION OF IONS AND ELECTRONS IN THE *B1* STRUCTURE

It is desired to compare the potential energy changes in the *B1* and *B3* structures, as electrons or Ag^+ or Br^- ions move along the lines of least resistance through them. These energy changes can be approximated by considering the electronic or ionic motions to occur without displacement or polarization of the other ions. This undoubtedly introduces considerable error, but the errors should be in the same direction and roughly of the same magnitude (or the same fraction of the total energy), at corresponding points in the two structures.

The ionic motions considered are those involved in the production of interstitial ions and in the motion of such ions from one interstitial position to another. Estimates of the net energy change when an ion moves from a normal lattice position to a distant interstitial position and of the magnitude of the energy hump between two interstitial positions have previously been made[7,8] for NaCl, KCl, and RbCl. Numerical comparison of these estimates with those deduced from the work reported here for AgBr will not be presented, because of the differences in the substances, because of important differences in the expressions used for the computation of the non-Coulomb energies, and because of the approximations, in the AgBr calculations, mentioned in the preceding paragraph.

The energies of interest are in part due to Coulombic and in part to non-Coulombic interactions. For the non-Coulomb part, we use Eqs. (1) to (3), summing over all the ions closest to the ion in question. To obtain the Coulombic contribution, we compute the Coulomb potential at appropriate points along the lines of motion in which we are interested and then multiply by the charge ($\pm e$) on the moving particle.

The treatment of an electron as a point charge, moving along certain fixed paths in the structure, is doubtless quantitatively inaccurate, but should give approximately correct relative values for the energy changes accompanying motion in the two crystal types being discussed or along different paths in either.

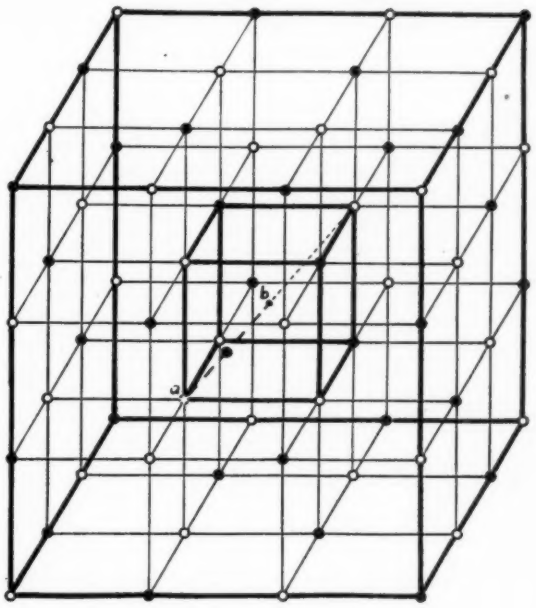

FIG. 3. Illustrating Højendahl's method of computing the potential at a point in a *B1* structure.

For the *B1* structure, we are interested in the motion of an Ag^+ or Br^- ion from its normal position along a cube diagonal to the center of an adjacent eighth-unit cube, also in the motion of an ion or electron from the center of one such small cube through one of its faces to the center of an adjacent cube (see Fig. 1).

The Coulomb potential, due to the other ions, at the center of any one ion in its normal position is $\pm\alpha e/a_0$, where α is Madelung's constant ($=3.4951$ for *B1*), e is the magnitude of the electron charge, and a_0 is the unit distance ($=2r_0$ for *B1*). The Coulomb potential at any point on the straight line connecting the centers of two adjacent cubes is zero, if no ions are missing or displaced from their normal positions. In case an ion is missing from the structure, the potential at a point on this line is $\pm e/d$, d being the distance between the vacant position and the point in question.

To obtain the Coulomb potential at a point on the diagonal connecting a normally occupied position with a cube center, we follow the method

[7] W. Jost and G. Nehlep, Zeits. f. physik. Chemie **B32**, 1 (1936).
[8] N. F. Mott and M. J. Littleton, Trans. Faraday Soc. **34**, 485 (1938).

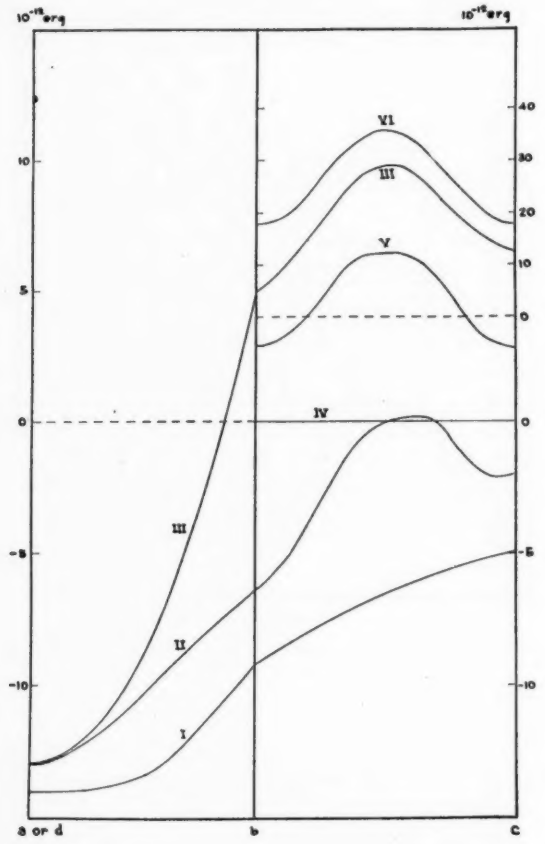

FIG. 4. Calculated energies for motion of an ion or electron in a *B1* type AgBr crystal along certain paths connecting points *a*, *d*, *b*, and *c* in the lattice (see Fig. 1). The ordinate scale at the upper right applies only to curves *VI* and *III* (between *b* and *c*). For further explanation, see Table III and the text.

used by Højendahl[9] in computing the Madelung constant. We sum $1/d$ directly, collecting together all the terms for ions at the corners of the eighth-unit cube containing the point for which the calculation is being made, then collecting all the terms for ions in the faces, edges, or corners of the next cubic box, concentric with the first, etc. (see Fig. 3). Three such boxes suffice to give an accuracy of better than 0.03.

Multiplying the Coulomb potentials, obtained as just described, by the magnitude of the electron charge gives the potential energy. This changes along the lines of interest as shown by curve *I* of Fig. 4.

[9] K. Højendahl, Kgl. Danske Vid. Sels. Math.-Fys. Medd. **16**, 133 (1938).

For the motion of a silver or bromide ion from a corner to the center of an eighth-unit cube or from one cube center to an adjacent one, the total energy—obtained by adding, to the Coulomb energy, terms for the non-Coulomb interaction with the closest other ions—varies as shown by the other lines in this figure.

POTENTIAL ENERGY CHANGES FOR MOTION OF IONS AND ELECTRONS IN THE *B3* STRUCTURE

The motions of interest in the *B3* structure are all along the body diagonals of the cubes. Besides the positions (a' and d', Fig. 1) normally occupied by ions, two types of normally unoccupied positions are of especial interest: (1) the b' positions, which are tetrahedrally surrounded by four Ag^+ ions, each at the distance r_0 (the same as the distance between closest ion centers), and (2) the c' positions, tetrahedrally surrounded by four Br^- ions, each at the distance r_0. The b' positions are at the centers of eighth-unit cubes, if the unit cell is so chosen that an Ag^+ ion is at each cell corner, or at the center and the centers of the edges of the unit cell, if it is so chosen that a Br^- ion is at each cell corner. Likewise, the c' positions are either at the center and the centers of the edges of the unit cell or else at the centers of half of the eighth-unit cubes, depending on the arbitrary choice of origin of the unit.

We are interested in the motion of an ion from its normal position (e.g., a') along the cube diagonal to the center (b') of an adjacent eighth-unit cube and then to the center (c') of the unit cell. We are also interested in the motion of ions and electrons along the cube diagonals (b' to c') in a *B3* structure in which no ions are missing from their normal positions.

The Coulomb potentials at points along the diagonals cannot readily be calculated by Højendahl's method. They have been computed, however, by a modification of Madelung's method.[10] We first choose an orthorhombic unit cell for the structure, with a diagonal of the cubic unit cell as the X axis of the new unit (see Fig. 5). The coördinates of the ions are listed in Table I.

We wish to calculate the potential at a point, $\bar{x}_0\,0\,0$, with x_0 having values between 0 and

[10] E. Madelung, Physik. Zeits. **19**, 524 (1918).

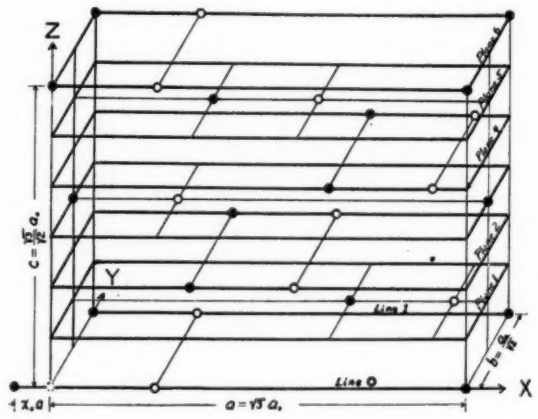

FIG. 5. Orthorhombic unit cell for the *B3* structure, used in calculation of the changes in Coulomb potential as an ion moves along a cube diagonal (=the X axis).

1/2. (The ion at the origin is assumed to have been removed.)

The Coulomb potential due to other ions in the X axis is given by the equation

$$V_0=\frac{e}{a}\Big[-\frac{1}{x_0+\frac{1}{4}}+16\sum_{m=1}^{\infty}\Big(-\frac{1}{16m-16x_0-4}+\frac{1}{16m-16x_0}+\frac{1}{16m+16x_0}-\frac{1}{16m+16x_0+4}\Big)\Big]. \quad (4)$$

Calculations for values of x_0 which are multiples of 1/16 are simple, since the denominators of the terms to be summed are all integers, and tables of reciprocals of integers are readily available.

We next consider the Coulomb potential at $\bar{x}\,0\,0$ due to other rows of ions, parallel to the X axis, in the XY plane. This is given, for the nth row on either side of the X axis, by the equation

$$V_n=\frac{4e}{a}\sum_{l=1}^{\infty}K_0(2\pi lrb/a)\cdot\{\cos(2\pi lx_0)-\cos[2\pi l(x_0+\tfrac{1}{4})]\}. \quad (5)$$

The function $K_0(x)$ is that tabulated by Jahnke and Emde[11] as $(i\pi/2)H_0^{(1)}(ix)$. A very small number of terms suffices.

[11] E. Jahnke and F. Emde, *Funktionentafeln mit Formeln und Kurven* (Teubner, Leipzig and Berlin, 1909), p. 135.

TABLE I. Coordinates of ionic centers, referred to the orthorhombic unit cell of Fig. 6.

Ag^+			Br^-		
x	y	z	x	y	z
0	0	0	1/4	0	0
2/3	1/2	1/6	11/12	1/2	1/6
1/3	0	1/3	7/12	0	1/3
0	1/2	1/2	1/4	1/2	1/2
2/3	0	2/3	11/12	0	2/3
1/3	1/2	5/6	7/12	1/2	5/6

TABLE II. Values of x, y and z for substitution in Eqs. (6), (7), and (8).

N	x	y	z
1, 7, 13	$2/3+x_0$	1/2	1/6
2, 8, 14	$1/3+x_0$	0	1/3
3, 9, 15	x_0	1/2	1/2
4, 10, 16	$2/3+x_0$	0	2/3
5, 11, 17	$1/3+x_0$	1/2	5/6
6, 12, 18	x_0	0	1

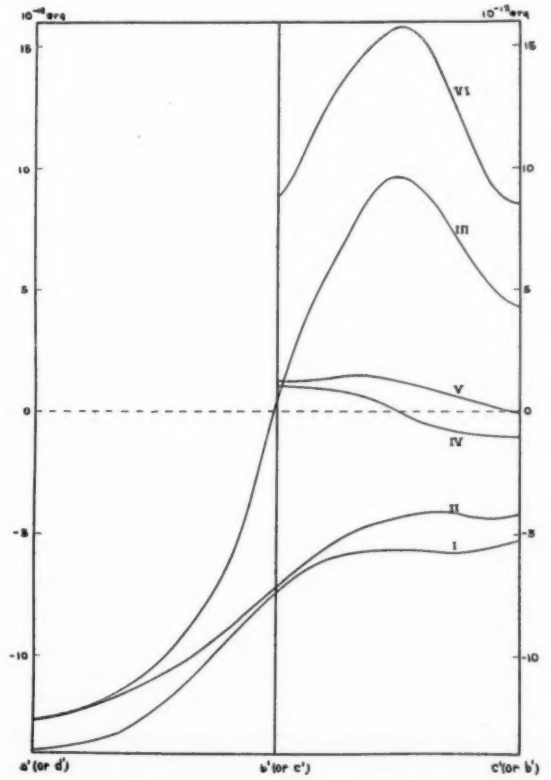

FIG. 6. Calculated energies for motion of an ion or electron in a *B3* type AgBr crystal along certain paths connecting points a', d', b', and c' in the lattice (see Fig. 1). For further explanation, see Table III and the text.

TABLE III. Summary of energy changes (in 10^{-12} erg), computed for undistorted structures and neglecting polarization

	Curves, Figs. 4 and 6	Net energy increase *B1*	Net energy increase *B3*	Activation energy *B1*	Activation energy *B3*
Motion of Ag^+ from normal position to nearest stable interstitial position.	*II*	10.9	8.3	13.2	8.5
Motion of Br^- from normal position to nearest stable interstitial position.	*III*	26	17	42	22
Motion of electron from one (most stable) interstitial position to another like it, in a complete lattice.	*IV*	0	0	0	2.1
Motion of Ag^+ from one (most stable) interstitial position to another like it, in complete lattice.	*V*	0	0	3.6	1.5
Motion of Br^- from one (most stable) interstitial position to another like it, in a complete lattice.	*VI*	0	0	18	7
Motion of Ag^+ from one of the interstitial positions of greater stability to one of those of lesser stability, in a complete crystal.	*V*	—	1.3	—	1.5
Motion of extra electron from an interstitial position in *B1* to one in *B3*.		−1.1			
Motion of extra Ag^+ from an interstitial position in *B1* to one in *B3*.		−2.8			
Transformation, *B1* to *B3* (per "molecule")		<0.4			

The Coulomb potential due to ions in the Nth plane, parallel to the XY plane, on each side of that through the origin, is

$$V_N=\frac{2\cdot 6^{\frac{1}{2}}e}{a}\{2\sum_l\sum_m K_{lm}\cos 2\pi my \times[\cos 2\pi lx-\cos 2\pi l(x+\tfrac{1}{4})] +\sum_l K_l[\cos 2\pi lx-\cos 2\pi l(x+\tfrac{1}{4})]\}, \quad (6)$$

where

$$K_{lm}=\frac{\exp[-2^{\frac{1}{2}}\pi z(l^2+6m^2)^{\frac{1}{2}}]}{(l^2+6m^2)^{\frac{1}{2}}}, \quad (7)$$

$$K_l=\frac{\exp[-2^{\frac{1}{2}}\pi zl]}{l}, \quad (8)$$

and x, y, and z have the values listed in Table II.

The total Coulomb potential due to all the ions in the lattice (other than that at 000) is

$$V'=V_0+\sum V_n+\sum V_N.$$

We have computed it for values of x_0 from 0 to 1/2, in multiples of 1/16. For $x_0=0$, we obtain $V'=-3.7829e/a_0$, the constant agreeing with the value of Madelung's constant for this structure.[12]

The addition of e/x_0a to the calculated values of V' gives the Coulomb potentials V at the points in question for the *complete* structure (including a positive ion at 000). As should be the case, V is symmetrical about $x_0=3/8$, where it is zero. (See curve *IV*, Fig. 6.)

[12] O. Emersleben, Physik. Zeits. **24**, 97 (1923).

At $x_0=0.25$, V has a positive value of $0.500e/a$ $(=0.2887e/a_0)$. A crystal having $a_0=6.305$A, with an electron in such a position, is $1.06\cdot 10^{-12}$ erg more stable than if the electron were not there or were in a position of zero potential. At $x_0=0.50$, V has the same magnitude, but is negative.

We now add to the Coulomb energy the sum of the non-Coulomb interaction energies for all the closest atoms (Fig. 2) to get the total energy for a silver or bromide ion at any given position on the cube diagonal. In Fig. 6 are curves showing how the total energy changes as an ion moves from its normal position (a') along a diagonal to nearby interstitial positions (b' and c'), also similar curves for motion of an *extra* ion or electron from one interstitial position (b' or c') to another, in a complete lattice. These curves are all computed for the interionic distance, $r_0=2.73$A (or $a_0=6.305$A).

SUMMARY AND CONCLUSIONS

The results of the calculations reported here are summarized in Figs. 4 and 6 and in Table III.

Corrections for polarization and distortion of the structure in the vicinity of extra ions, extra electrons, and vacant normally-occupied positions would probably decrease all the net energy increases and activation energies in this table. The approximate relationship between the *B1* and *B3* values should not be markedly affected, however.

It should also be remarked that the energy

changes indicated for the motion of an electron through either structure do not include any "overlap" energy of repulsion between the electron and neighboring atoms, nor is any consideration given to possible discrete energy levels for this electron. An electron moving through a *B1* type structure passes much closer to other atoms than one moving through a *B3* structure; this might result in a considerably larger "activation energy" hump in the former case than in the latter.

From the results of these calculations, it seems safe to draw the following conclusions:

1. For a perfect crystal, the *B3* structure is slightly less stable than the *B1* structure. This relationship may be reversed, however, in the vicinity of an extra Ag^+ ion or an extra electron, or both.

2. Ionic conduction through both structures is by Ag^+ ions, not by Br^- ions.

3. The ionic conductivity of the *B3* structure is considerably greater than that of the *B1* structure, at the same temperature.[13]

4. Extra electrons and extra ions "prefer" the *B3* structure to the *B1* structure.

[13] It may be noted that AgI, with a *B3* or *B4* structure, is a much better conductor than AgBr, with a *B1* structure, at the same temperature.

THE JOURNAL OF CHEMICAL PHYSICS VOLUME 11, NUMBER 9 SEPTEMBER, 1943

The Photographic Latent Image

II. Outline of the Theory*†

MAURICE L. HUGGINS
Eastman Kodak Company, Rochester, New York

(Received April 12, 1943)

A theory of the formation and growth of the photographic latent image and of the development process in the crystal containing it is outlined. It is assumed that the latent image consists of a small region of the (silver halide) crystal in which the atomic arrangement is the "tetrahedral" *B3* type (or another closely related arrangement), stabilized by the presence of one or more photoelectrons, with or without extra silver ions.

INTRODUCTION

WHEN a silver bromide crystal held in a gelatin layer is exposed to light, some change occurs, as a result of which a developing solution can attack the crystal and reduce it to metallic silver more easily than if it had not been exposed to light. In photographic literature, a crystal which has suffered this change is said to contain a *latent image*. Many theories have been suggested as to the nature of the change which occurs.[1] That most generally accepted at the present time is due to Gurney and Mott.[2,3] According to this theory, the initial effect of light is to liberate photoelectrons in the silver bromide lattice. These move to specific points and produce a negative charge at those points. Silver ions then move through the lattice; when they reach the charged points they are neutralized, forming a metallic silver nucleus. This silver nucleus, it is assumed, constitutes the latent image, which makes the crystal more readily developable than it would be otherwise.

The purpose of the present paper is to suggest an alternative theory, according to which the latent image consists not of crystalline metallic

* Presented before the Division of Physical and Inorganic Chemistry at the Detroit Meeting of the American Chemical Society, April 12, 1943.

† Communication No. 922 from the Kodak Research Laboratories.

[1] C. E. K. Mees, *The Theory of the Photographic Process* (Macmillan, New York, 1942).

[2] R. W. Gurney and N. F. Mott, Proc. Roy. Soc. **164A**, 151 (1938).

[3] J. H. Webb, J. App. Phys. **11**, 18 (1940).

silver but of a small region of the crystal or crystal surface in which the atomic arrangement is that known as *B3* or cubic ZnS type (or some other closely related arrangement), stabilized by the presence of extra electrons (photoelectrons), perhaps with extra silver ions also.

LATTICE ENERGIES

AgCl and AgBr crystals normally have the NaCl or *B1* type of structure,[4] in which each ion is surrounded equidistantly by six ions of the other kind. AgI crystallizes in either of the two closely related "tetrahedral" structures,[4] *B3* (cubic) and *B4* (hexagonal), in each of which each ion is surrounded tetrahedrally by four of the other kind. (For diagrams of the unit cubes of the *B1* and *B3* structures, see Fig. 1 of the preceding paper.[5]) AgBr and AgI form solid solutions, having the *B1* structure if the iodide concentration is low, the *B3* or *B4* structure if it is high, and either or both structures within an intermediate range.[6]

The lattice energies of the *B3* and *B4* types of structure are very nearly the same. For simplicity in description, we shall consider, in the remainder of this paper, only *B3* (of these two). It should be understood, however, that nearly all that is stated with regard to *B3* would also apply to *B4*.

From the facts just noted about the structures of AgBr and AgI and their solid solutions, one would expect the lattice energies of a *B1* type AgBr crystal and of a hypothetical *B3* type AgBr crystal to differ but slightly. Calculations of these energies,[5,7] by methods which have previously yielded results in good agreement with experiment, show this to be the case. The lattice energies for the two structures should be even more nearly equal for silver bromide containing a small amount of iodide, as in many photographic emulsions. The preference of the iodide for the tetrahedral structures may be explained as due to the greater tendency of iodine (than of bromine) to form covalent bonds with silver. Electron-pair bonds between all adjacent atoms are possible in the *B3* and *B4* structures,[8] but not in the *B1* structure, the number of valence electrons being insufficient.

The *B3* structure, unlike the *B1* structure, contains "holes" of positive potential and other "holes" of negative potential (see Fig. 1). The former are possible sites for extra electrons (e.g., photoelectrons). From the calculations of the preceding paper, we may conclude that an electron in such a site stabilizes the structure by at least $1 \cdot 10^{-12}$ erg or 0.6 electron volt. *The presence of extra electrons therefore favors the transition from a B1 to a B3 structure.*

The holes of positive (and negative) potential in the *B3* structure are also possible sites for extra negative (and positive) ions. Extra ions (if not too large) would fit into the crystal structure without introducing large overlap repulsion energies. An extra Ag^+ ion, for instance, would have as nearest neighbors four tetrahedrally disposed Br^- ions, these closest ions being arranged just like those around each of the other similar normally placed ions in the structure.

Extra ions cannot fit into the *B1* structure without producing large repulsion energies. From the data in the preceding paper, one may compute $2.9 \cdot 10^{-12}$ and $0.15 \cdot 10^{-12}$ erg as the increase in energy (decrease in stability) resulting from the insertion of an extra Ag^+ ion in the *B1* and *B3* structures, respectively. Allowance for polarization and shifts of the surrounding ions would decrease these instability energy values somewhat; the actual *B3* energy change is, in all probability, negative, the structure being more stable with the extra Ag^+ ion than without it. (Many extra Ag^+ ions cannot be present, without compensating extra electrons or negative ions, because of the Coulomb energy produced by their mutual repulsions.)

Similar calculations indicate that the chance of having extra Br^- ions in either type of structure is negligible, except possibly at the surface of a *B3* structure, where large displacements can occur. Additional Br^- ions might well be adsorbed at otherwise vacant surface sites of positive potential.

One may conclude from the foregoing that extra Ag^+ ions within the crystal or extra Ag^+ ions or (possibly, to a lesser extent) Br^- ions on the surface tend to make the *B3* structure more

[4] P. P. Ewald and C. Hermann, *Strukturbericht, 1913–1928* (Akademische Verlagsgesellschaft, Leipzig, 1931).
[5] M. L. Huggins, J. Chem. Phys. **11**, 412 (1943).
[6] R. B. Wilsey, J. Frank. Inst. **200**, 739 (1925).
[7] J. E. Mayer, J. Chem. Phys. **1**, 327 (1933).
[8] M. L. Huggins, J. Am. Chem. Soc. **44**, 1841 (1922).

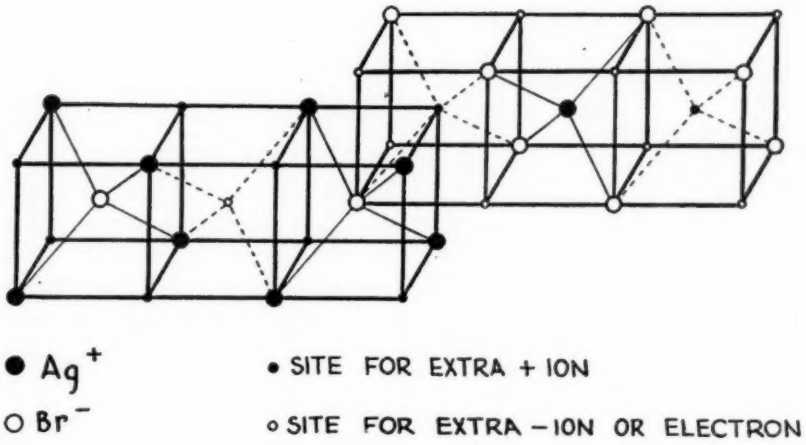

FIG. 1. A portion of the *B3* structure, showing (small dots) possible sites for extra positive ions and (small open circles) possible sites for extra negative ions or electrons.

stable than the *B1* structure, in their immediate vicinity.

Extra ions of other sorts—especially those having high polarizabilities and tendencies to form covalent bonds but with radii about the same or smaller than that of Ag^+—should similarly favor the *B3* structure. Particularly effective should be the substitution of a bivalent positive ion, such as Hg^{++}, for some of the Ag^+ ions, along with extra electrons—one for each substitution, if the crystal remains electrically neutral. The addition of mercury atoms (Hg^{++} plus two electrons) to the surface of a silver halide crystal would certainly favor the transition from *B1* to *B3* in the adjacent positions of the crystal. This may well be the cause of various hypersensitivity effects produced by mercury vapor.

Similar reasoning leads to the conclusion that the replacement of some of the Br^- ions by S^{--} ions, either within the crystal or on the surface, should also make the transition from *B1* to *B3* energetically easier. For neutrality, there should be one extra positive ion (Ag^+) for each Br^- ion so replaced, each extra ion helping to make *B3* more stable than *B1*.

One would, in fact, expect a sulfide ion (in the crystal interior) to tend to produce a *B3* type structure with *two* (or perhaps more) extra Ag^+ ions around it, in addition to those normally around each negative ion. This region would attract extra electrons (e.g., photoelectrons) to nearby positive potential holes. Perhaps the transition to this modified *B3* structure would occur only if and when such extra electrons are available. The structure at and immediately surrounding the S^{--} ion, according to this picture, can properly be described as a "silver sulfide speck." (The Ag_2S and AgBr structures are not separated by a distinct boundary, but are coherent; some of the silver ions are common to both.) The hypothesis under discussion thus furnishes a reasonable explanation for the marked sensitizing effect, discovered by Sheppard,[9] of sulfide compounds which are capable of producing silver sulfide during the making of the photographic emulsion.

The adsorption of polar dyes onto the surfaces of a silver bromide crystal has several effects which are pertinent to the present discussion: (1) By occupying surface sites which would otherwise be occupied by Br^- or other negative ions, each adsorbed dye molecule or ion produces a region of excess positive charge—as compared with other surface regions, at least. This is especially true if the adsorbed dye is a positively charged ion. (2) Because of the positive charge in this region, extra electrons (photoelectrons and developer electrons) are attracted to it. (3) The presence of extra electrons tends to transform this region to a *B3* type structure. The composition of the dye may also be such as to favor this

[9] S. E. Sheppard, Phot. J. **65**, 380 (1925).

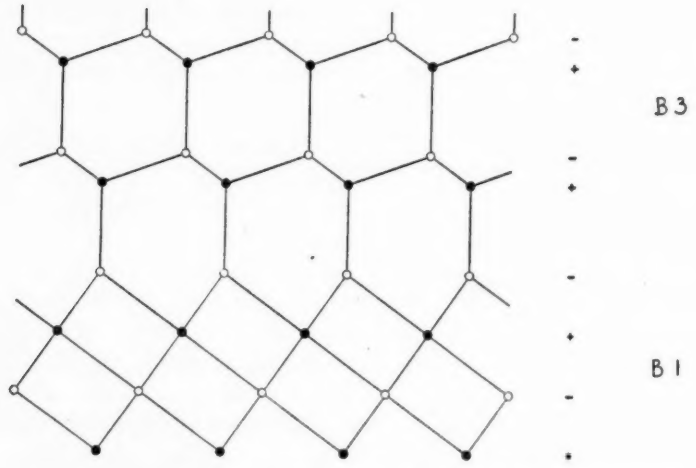

FIG. 2. Projection, onto a {110} plane, of a crystal, the upper portion of which has the *B3* structure, the lower portion the *B1* structure. {111} planes are horizontal, in both structures.

transformation. (4) Absorption of light by the dye molecule or ion releases an electron, either from the dye or from an adjacent Br^- ion, in the very place where it would be most effective in producing a *B1*-to-*B3* transformation. (5) In the vicinity of the adsorbed dye molecule or ion, the potential barrier hindering the approach and adsorption of developer ions is less than elsewhere on the crystal surface, because the net charge density is less negative than elsewhere.[10,11]

For several reasons, therefore, one would expect adsorbed dyes to have a photosensitizing effect, as they do. Obviously, different dyes should differ as regards their effectiveness.

RELATIVE DIMENSIONS

Unit cells of the *B1* and *B3* structures contain the same number (4 each) of Ag^+ and Br^- ions. The unit distance a_0 computed for *B3* is about 6 percent larger than the experimental value[4] of a_0 for *B1*. The calculated *B3* value might be in error, perhaps, by 2 or 3 percent, but probably not more.

The replacement of some of the Br^- ions by I^- should tend to make the *B1* and *B3* dimensions a little more nearly equal. The presence of extra Ag^+ ions might have a slight effect in the same direction. Extra electrons in the structure, however (especially with extra Ag^+ ions also present), would have a much more marked effect. For a definite, but unknown, concentration of extra electrons (or of extra electrons plus extra Ag^+ ions), a transformation from *B1* to *B3* could take place without any change of dimensions. It could occur even in the interior of a single crystal, without breaking up the crystal structure.

At the surface of a crystal there is necessarily considerable strain, because the environment of the surface atoms is not the same as that of atoms in the interior. This surface strain would be relieved somewhat if the surface atoms were in a structural arrangement which, under similar circumstances, would be slightly less dense. Provided a suitable transition is possible between the two structure types (see below), we might therefore expect a *B3* type surface on a *B1* crystal. Other factors, especially the nature of the environment outside of the crystal (adsorbed ions, etc.), are also important, however. It may be that the surface of a crystal in a photographic emulsion contains regions of both types, *B1* and *B3*, or that the surface is all of the *B1* type but in certain areas (sensitivity specks) can easily change to the *B3* type on the addition of extra electrons.

THE TRANSITION FROM *B1* TO *B3*

The distribution of bromide ions, considered by themselves, is precisely the same for a *B3* and

[10] R. M. Evans and W. T. Hanson, Jr. Phot. J. **77**, 497 (1937).
[11] T. H. James and G. Kornfeld, Chem. Rev. **30**, 1 (1942).

for a *B1* structure. If the dimensions are also the same, we may picture a single crystal as being in part *B1* and in part *B3*, the Br^- ion distribution being continuous throughout the whole, only the distribution of Ag^+ ions and extra electrons being different in the two parts. The structure in a portion of such a double-type crystal is represented in Fig. 2. There is no sharp break between the two structures, one sheet of Br^- ions being common to both. Where the two structures come together, as well as within each structure, the arrangement of ions is energetically reasonable.

For simplicity and clarity, the boundary between the two structures in this figure follows a definite {111} plane. This need not actually be so; an irregular boundary would be quite possible. The boundary between the two structures could shift very readily, one atom at a time. An Ag^+ ion on the *B1* side of the boundary need shift only slightly, as shown in Fig. 3, in order to take its place as a portion of the *B3* part of the crystal, the shift involving only a very small activation energy (less than 10^{-12} erg). Moreover, the presence of extra electrons in the *B3* region would result in an attraction for the Ag^+ ions on the *B1* side of the border and would make this energy hump still smaller.

Extra electrons in any region of a crystal (over the number required to balance any excess positive charge which may previously have existed there) would attract positive ions, causing a (slow) migration in that direction of any interstitial Ag^+ ions present in the vicinity. From the calculations of the preceding paper, it follows that equilibrium concentration of interstitial ions in a *B3* region is considerably greater than that in a *B1* region, also that the rate of migration of such ions through a *B3* structure is considerably faster than that through a *B1* structure. At any rate, an extra electron would before long be neutralized by an extra Ag^+ ion near it, occupying one of the close sites of negative potential. This process prevents the accumulation in a *B3* latent image of an excess negative charge—which would repel additional photoelectrons.

Even after "neutralization" by an extra Ag^+ ion, an interstitial electron in a *B3* structure would still attract (over small distances) other interstitial Ag^+ ions and, in time, would be expected to hold a second such ion in the immediate vicinity. This region would then have a net *positive* charge, making it (like the original sensitivity speck) an attractive center for more photoelectrons or developer ions.

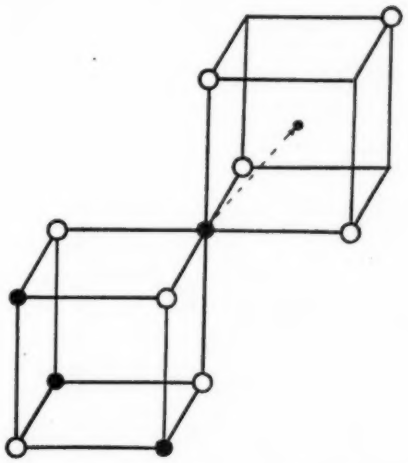

FIG. 3. Illustrating the nature of the shift made by a silver ion when it leaves the *B1* structure on one side of a *B1–B3* boundary to become part of the *B3* structure on the other side.

Reciprocity law failure at high intensities may be attributed to the accumulation of photoelectrons in a *B3* region faster than they can be neutralized by Ag^+ ion migration or faster than the potential resulting from the charge can be attenuated by growth of the *B3* region at the expense of *B1*. Reciprocity law failure at low intensities may be ascribed to slow diffusion of captured electrons from *B3* regions, or to regression of the *B3* region after neutralization by Ag^+ ions of the charges of the excess electrons therein (or, even more, after the acquisition of more Ag^+ ions than enough to neutralize the photoelectrons).

The Herschel effect may be attributed to the photoelectric ejection of extra electrons in a *B3* latent image region. This would cause the *B1–B3* boundary to shift in such a direction as to decrease the size of the *B3* region or to eliminate it entirely.

DEVELOPMENT

The process of development of a silver halide grain consists essentially of the addition of electrons and the removal of halide ions. Both optical

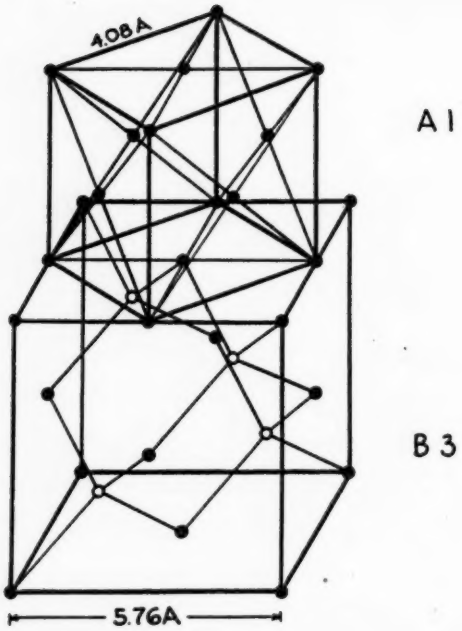

FIG. 4. Illustrating the formation of a metallic silver crystal (*A1* structure) on a {100} face of a *B3* AgBr crystal.

microscope studies[12,13] and electron microscope studies[14–16] have shown that in some cases the metallic silver produced by development grows outward from the silver halide crystal surface. The places at which these growths start from the crystal may reasonably be assumed to be latent-image regions.

A *B3* latent image region at the crystal surface can be assumed to have a lower potential barrier, resisting adsorption of electronegative developer ions, than a *B1* surface region (covered by negative ions) for several reasons: (1) There is probably little or no excess of negative ions on the *B3* surface, as already noted. (2) At the surface, as in the interior, a *B3* structure has sites of positive potential—other than those at the normal ion positions—which would attract close negative ions; this is not true of a *B1* structure. (3) As a result of the tendency of each extra electron in a *B3* structure to accumulate one or more extra Ag^+ ions in the immediate neighborhood, each *B3* region would (sometime after exposure) either be neutral or (more probably) positively charged. (4) The extra electrons—and, to a lesser extent, the extra Ag^+ ions—in a *B3* region are very mobile, shifting readily on the approach of another charged particle. In other words, a *B3* latent image is readily polarized on the approach of a developer ion, this polarization producing an attraction. A *B1* region is not readily polarized.

On adsorption of a developer ion to a *B3* surface, the former gives up an electron to the latter. Extra electrons entering the *B3* lattice in this way attract silver ions from below the surface, pulling them over energy humps which are small, to previously unoccupied sites of negative potential in and near the surface. *This produces a distribution of silver kernels in the {100} planes exactly like the distribution in a {100} plane of metallic silver, even as regards dimensions.*[17] (See Fig. 4.) A surface of this sort may quite properly be described as a surface of metallic silver.

Additional developer ions might be adsorbed to such a silver surface even more readily than to a *B3* surface. Whether or not that is the case, continued action of the developer furnishes more electrons, which move toward this region of excess silver kernels. As the concentration of electrons builds up, a second sheet of silver kernels is formed, outside of the first, the ions going to the energetically most favorable sites, at

[12] W. Scheffer, Brit. J. Phot. **54**, 116, 271 (1907).
[13] C. Tuttle and A. P. H. Trivelli, Phot. J. **68**, 465 (1928).
[14] M. von Ardenne, Zeits. f. angew. Phot. **2**, 14 (1940).
[15] C. E. Hall and A. L. Schoen, J. Opt. Soc. Am. **31**, 281 (1941).
[16] F. F. Lucas, see reference 1, p. 834.

[17] The simple relationship existing between the dimensions of metallic silver and those of ordinary (*B1*) silver bromide has been noted by J. J. Trillat and H. Motz, J. de phys. et rad. [7] **7**, 89 (1936), by P. D. Dankov, Comptes rendus U.R.S.S. **24**, 733 (1939), by P. D. Dankov and A. A. Kochetkov, *ibid.*, **26**, 785 (1940), and by H. Wilman, Proc. Phys. Soc. London **52**, 323 (1940). Dankov's assumed mechanism for the formation of a metallic silver crystal on the surface of a *B1* AgBr crystal, however, is more complicated and less reasonable than the mechanism postulated here for the production of a silver crystal on a *B3* AgBr crystal. Wilman showed by electron diffraction methods that reaction of halogen vapors on thin silver films produced silver halide crystals which were oriented, relative to the underlying silver structure, in the manner indicated in Fig. 4. For simplicity of description it is assumed, in Fig. 4 and in the explanation (in the text) of the formation of a silver crystal on a silver halide surface, that the former starts at a {100} surface of the latter. That is not theoretically necessary, however. Oriented growth of a silver crystal on a {111} surface of a silver bromide crystal would seem to be especially likely, since the arrangement of silver kernels in a {111} face of a *B3* (or *B1*) silver bromide crystal is just the same, even as regards dimensions, as that in a {111} face of a metallic silver crystal.

points opposite the centers of the squares of the underlying silver layer. They may reach these sites by migration along the crystal surface from points where they are least tightly held, or they may come from the previously formed silver layer, the sites vacated being soon refilled by other like ions migrating (because of the potential gradient) from the crystal interior. Under certain circumstances, silver ions might also be deposited from the solution.[10,11]

Continuation of this process produces a silver crystal growing *outward* (possibly also spreading sideways, under suitable conditions) from the original surface, the two structures fitting together as indicated in Fig. 4. Without sideways growth, a filamentary structure would thus be produced.

The growth of the silver crystal is necessarily accompanied by diffusion of electrons, either from it or directly from the developer ions, into the *B3* crystal, also by growth of the *B3* region at the expense of the *B1* part of the crystal.

In view of the considerably higher activation energy for motion of a silver ion through a *B1* structure than through a *B3* structure,[5] it seems probable that such motion occurs only in the *B3* regions or along a *B1* (or *B3*) surface. The migration of the Ag^+ ions continually diminishes the forces holding the surface bromide ions. These, therefore, become free to diffuse, more or less readily depending on the composition of the solution and the nature of the surface, into the solution.

Very long exposure to light, in spite of the growth of the *B3* regions and the migration of Ag^+ ions, must eventually cause the negative charge on these regions to build up, eventually resulting in the formation and growth of metallic silver crystals, as when the extra electrons are supplied by the developing agent. Uncharged bromine atoms and, from them, bromine molecules are of course produced at the same time.

SUMMARY

The processes involved in latent image formation and growth and in subsequent development of the crystal grain may be outlined as follows:

1. Absorption of a light quantum by an atom (usually Br^-) produces a photoelectron.

2. Unless recaptured by the atom from which it came (or some other uncharged bromine atom), the photoelectron diffuses through the crystal until it settles in a site having a positive potential somewhat greater than that at any point within the normal structure. Such sites (sensitivity specks) will usually be at the crystal surface, near ions or molecules of particular kinds adsorbed on its surface. Regions containing sulfide ions surrounded by extra silver ions ("silver sulfide"), mercury ions with or without extra electrons ("metallic mercury"), extra silver ions with or without extra electrons ("metallic silver"), and crystal surface areas covered by appropriate adsorbed dye ions (instead of the extra halide ions elsewhere on the surface) would be expected to be especially effective in attracting and trapping photoelectrons.

3. Cooperation between the electron and these foreign ions or molecules produces a shift, over a limited region in the immediate vicinity, from the normal *B1* type of structure to a *B3* (or similar) type. The transformation involves only slight movement of the silver ions.

4. Any net negative charge produced in a *B3* region by the addition to it of (one or more) photoelectrons is slowly neutralized by the migration of silver ions toward these electrons. Further migration and accumulation of Ag^+ ions around each electron may even give the region a net negative charge. Conditions are then favorable for the further addition of more photoelectrons or for development.

5. Additional photoelectrons finding their way to this *B3* region produce further shifts of silver ions at the *B3–B1* boundary, thereby causing this boundary to shift in such a way as to increase the size of the *B3* region.

6. In the development process, extra electrons from the developer enter the surface of a *B3* region (more readily than that of a *B1* region). After development has started, they may also enter at the silver surface. These electrons diffuse into the interior of the *B3* region, causing it to expand at the expense of the *B1* part of the crystal, as outlined in (5).

7. The extra electrons also produce migration of silver ions—especially in the *B3* structure and along the crystal surface, both where the

underlying structure is *B3* and where it is *B1*—in such a way as to start a crystal of metallic silver on the surface.

8. Further additions of migrating silver ions cause this silver crystal to grow. Because of the difficulty of concurrent migration of bromide ions away from the silver crystal, the latter usually grows *outward* from the original surface of the silver halide crystal, producing the filamentary structure observed.

9. The ionic migrations just described leave the bromide ions on the surfaces held only very loosely or not at all; the excess negative charge within the crystal in fact repels them. They therefore diffuse away into the solution, at a rate depending on the nature of the solution, on the rate at which electrons are being supplied to the crystal aggregate by developer ions, and on the rate of migration of silver ions within the aggregate.

It should be emphasized that in none of the assumed processes is any break-up and reformation of crystals necessary: both the transition from *B1* to *B3* and that from *B3* to metallic Ag are continuous. The *B3* structure "catalyzes" the development process by making it possible for the addition of electrons from the developer, the formation and growth of silver crystals, and the removal of Br^- ions from the silver halide crystal all to occur at different, not necessarily adjacent, locations.

In conclusion, the writer takes pleasure in acknowledging the help received from discussions of this subject with other members of the Kodak Research Laboratories staff, especially Drs. S. E. Sheppard, T. H. James, and J. H. Webb.

THE JOURNAL OF CHEMICAL PHYSICS VOLUME 11, NUMBER 9 SEPTEMBER, 1943

X-Ray Diffraction Investigation of Sodium Stearate from Room Temperature to the Melting Point

A. DE BRETTEVILLE, JR.,* AND J. W. McBAIN
Chemistry Department, Stanford University, Stanford University, California

(Received March 11, 1943)

Sodium stearate of the gamma-polymorphic form was photographed by Cu $K\alpha$ x-rays in a powder camera at seven temperatures between room temperature and 301°C. The long spacing is constant up to 132°C, the transition temperature between the subwaxy and waxy phases, whereupon it continues to decrease markedly in length up to the melting point. The two most intense short spacings increase in length up to about the transition between the stable waxy crystalline phase to superwaxy phase at 167°C. Both lines then appear to coalesce to form a single line up to above the final melting point, from liquid crystal to liquid, at 288°C. The space lattice was assumed to be monoclinic over the whole temperature range studied, with hexagonal close packing of the chains themselves above 167°C, possibly as a result of molecular rotation of the chains about their axes.

INTRODUCTION

SODIUM stearate exhibits seven stable phases between room temperature and the melting point at 288°C.[1,2] The phase changes are given in Table I.

The successive changes of sodium stearate on warming have been observed by the dilatometer method,[3] the hot wire method of I. Fankuchen with crossed Polaroids, or with the "mikropolychromar" microscope,[2] and the calorimetric method,[1] and it was thought the x-ray diffraction method would give additional information.

The gamma[4–6] polymorphic form was used in

* Present address: 64 Terrace Road, Medford, Massachusetts.

[1] R. D. Vold, J. Am. Chem. Soc. **63**, 2920 (1941).

[2] M. J. Vold, M. Macomber, and R. D. Vold, J. Am. Chem. Soc. **63**, 168–175 (1941).

[3] R. D. Vold and M. J. Vold, **61**, 808–816 (1939).

[4] A. de Bretteville, Jr., and J. W. McBain, Science **96**, 470–471 (1942).

[5] M. J. Buerger, L. B. Smith, A. de Bretteville, Jr., and F. V. Ryer, Proc. Nat. Acad. Sci. **28**, 526–529 (1942).

[6] J. W. McBain, A. de Bretteville, Jr., and S. Ross, J. Chem. Phys. **11**, 179–183 (1943).

this investigation. It may be obtained by heating the hydrated alpha-form in an *open* tube, where it changes to the beta-form at 54°C and then to the supercurd phase (stable between 89°C and 114°C); thereafter the stearate reverts to the gamma-form, which is the most stable form at room temperature. The gamma-form exhibits at room temperature the same long x-ray spacing, even when it has been obtained by cooling sodium stearate from above the melting point. W. W. Lee has shown that sodium stearate forms a hemihydrate when exposed to half-saturated water vapor.[7] However, all fibrous forms of soap sorb water in a continuous manner, depending upon the relative humidity. Hence any actual analytical composition (other than the hemihydrate) is devoid of significance. McBain, Boldnan, and Ross[8] have presented an x-ray examination of the hydrated gamma-form of sodium stearate.

EXPERIMENTAL METHOD

A circular x-ray heating camera[9] of the pinhole type, was used to take pictures at successively increasing temperatures of the sample. The sodium stearate used was made from Kahlbaum acid by Dr. E. L. McBain.[10] The sample to film

TABLE I.

Phase	Temperature	Method
curd-supercurd	90°C	dilatometer, x-rays
subwaxy	117°C	dilatometer, x-rays
waxy	132°C	dilatometer, hot wire
superwaxy	167°C	dilatometer, hot wire
subneat	205°C	dilatometer, hot wire
neat	257°C	dilatometer, hot wire
isotropic [liquid]	288°C	dilatometer, hot wire, visual observation, microscope

radius was 5.73 cm. The sample was sealed in clear radio code No. 707 Corning glass not over 1-mm inside diameter and rotated at 1 r.p.m. Cu $K\alpha$ radiation was obtained from a copper x-ray tube with a thin Pyrex "bubble window"

[7] W. W. Lee, Ph.D. Thesis, Stanford University, (1941). Obtainable in bibliofilm from the U. S. Department of Agriculture. J. W. McBain and W. W. Lee, Ind. Eng. Chem. **35**, 784 (1943).

[8] J. W. McBain, O. E. Boldnan, and S. Ross, J. Am. Chem. Soc. (in press).

[9] Rev. Sci. Inst. **13**, 481–483 (1942); J. App. Phys. **14**, 137 (1943).

[10] E. L. McBain, J. Phys. Chem. **44**, 1014 (1940).

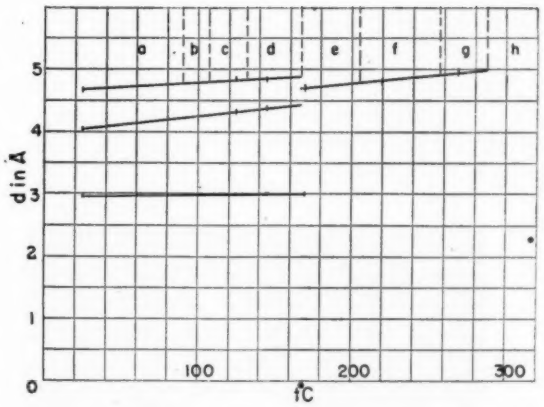

FIG. 1. Short spacings in angstrom units as a function of temperature. The phases are bounded by the dashed lines, and are designated by: *a*(curd); *b*(supercurd); *c*(subwaxy); *d*(waxy); *e*(superwaxy); *f*(subneat); *g*(neat); *h*(isotropic liquid).

made by James F. Lee,** under a grant furnished through the Cyrus M. Warren Fund. The radiation was filtered by 0.01-cm foil of electrolytic nickel. The voltage applied to the tube was 28 kv at 28 ma. The exposure time was 2 hours.

The photographs were measured visually with a sliding cross hair and vernier reading to $\frac{1}{10}$°.

EXPERIMENTAL RESULTS

Figure 1 shows the short spacings d, as a function of the temperature. These data were obtained from the photographs shown in Fig. 2. Starting from room temperature the two most intense side spacings increase in length and in diffuseness as the temperature increases. This diffuseness may be due to decreased alignment because of the release of constraint with increasing temperature. Finally these two lines appear to merge above 170°C in the superwaxy phase (167°C–205°C).

The long spacing d is tabulated in Table II as a function of temperature. The long spacing begins to decrease at 145°C in the waxy phase (132°C–167°C) and continues to decrease as the temperature increases. The value at 301°C in the isotropic phase is the mean of results of measurements on oriented doublets of the second and third orders. The doublets are short sharp arcs, in the 9 and 3 o'clock positions on the photograph, parallel to the axis of the sample capillary.

** 193 Willow Road, Palo Alto, California.

The oriented doubling may be due to the fact that a thin layer of molecules near the capillary walls is oriented. R. D. and M. J. Vold noticed that the soap becomes oriented in the isotropic liquid and neat phases between glass cover plates used in the hot wire method.[11]

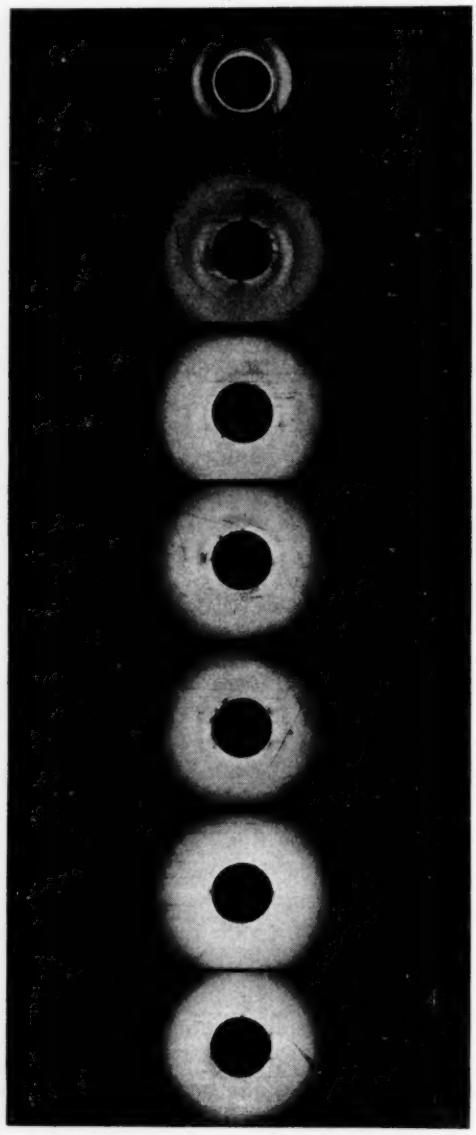

FIG. 2. Successive changes of sodium stearate diffraction pattern (θ range 0°–44°) with increase of temperature. The photographs show temperatures at: (a) room; (b) 125°C in the subwaxy phase; (c) 145°C in the waxy phase; (d) 170°C in the superwaxy phase; (e) 220°C in the subneat phase; (f) 269°C in the neat phase; (g) 301°C in the isotropic liquid.

[11] See reference 3, p. 171.

TABLE II

T°C	d(A)	n(order)	Intensity
25°C	44.3	5	s
	44.9	7	w
	4.68		m
	4.05		s
	2.95		w
125°C	44.7	3	m
	4.83		w
	4.30		s
	2.97		w
145°C	42.9	3	s
	4.81		m
	4.36		s
	2.99		w
170°C	39.9	3	m
	4.68		m
	2.98		vw
220°C	37.9	2	s
	38.3	3	s
	4.78		m
269°C	34.0	2	s
	33.3	3	m
	4.92		m
301°C	31.9	2	s
	32.3	3	m
	4.82		w

DISCUSSION

Powder diffraction data are given in references 4 and 6, and the fiber diagram with derived unit cell in reference 8 for the gamma-form of sodium stearate at room temperature. The alpha-lattice was investigated by M. J. Buerger with single hydrated crystals of sodium stearate and sodium palmitate grown by A. de Bretteville, Jr., and F. V. Ryer.[12] It has monoclinic symmetry. Crystals of the beta-form obtained by heating the alpha to 54°C are shattered and opaque and poorly suitable for analysis. P. A. Thiessen and J. Stauff characterized the beta-form as monoclinic,[13] and McBain, de Bretteville, and Ross used their rotation photograph to index correctly the beta-powder photograph.

As shown in Table II, the long spacing decreases as the temperature increases, especially above about 132°C. This may be attributed to an increase of tilt of the chains. The length of the *c* axis is uncertain, because for a monoclinic

[12] M. J. Buerger, Proc. Nat. Acad. Sci. **28**, 530 (1942).
[13] Zeits. f. physik. Chemie **A176**, 397 (1936).

space lattice the long spacing is $c \sin \beta$, where c, the length of the c axis, and β, the angle of inclination of this axis with respect to the basal plane, are both unknown. However, if the double molecules of length 52.1A lie in the c direction, the value of β would be about 60°. Then, taking also the increase in side spacing into account, the x-ray data would confirm the dilatometer results that as the temperature is raised the specific volume of each successive phase is larger.

Hexagonal cylindrical packing inclined at an angle to the basal plane might result from spinning of the carbon chains about their axes at high temperatures in the phases above 167°C. The subwaxy and the waxy phase are definitely crystalline, but the superwaxy phase, existing between 167° and 208°C, more nearly resembles the liquid crystalline forms subneat (208°–238°) and neat (238°–288°). It is probable that in these three forms the dipole carboxylate groups are fixed with respect to each other while the paraffin chains rotate on their axes. The inclination of the axes must result from the fixation of the carboxylate heads which largely determine the angle of the single bond holding the paraffin chain.

It may be noted that the analogous normal-paraffins also exhibit numerous phase changes below their m.p. with hexagonal cylindrical packing above the m.p., as shown by A. Müller.[14]

[14] A. Müller, Proc. Roy. Soc. **A138**, 514–530 (1932).

Letters to the Editor

PROMPT publication of brief reports of important discoveries in physics may be secured by addressing them to this department. The closing date for this department is the third of the month. Because of the late closing date for the section no proof can be shown to authors. The Board of Editors does not hold itself responsible for the opinions expressed by the correspondents. Communications should not in general exceed 600 words in length.

An Absolute Method for the Determination of the Area of a Fine Crystalline Powder

WILLIAM D. HARKINS AND GEORGE JURA
University of Chicago and Universal Oil Products Company, Chicago, Illinois
July 12, 1943

PRIOR to the development of the methods presented here in three letters, there has been only one reliable method for the determination of the area of a solid in the form of thin sheets, of a powder, or a porous material. That method, developed by Emmett, together with Brunauer and Teller,[1] is based on an isotherm (*BET*) which does not give an area, but only the volume (v_m) of gas adsorbed upon the surface of the solid to form a complete monolayer. From this, the number (N) of molecules in the monolayer may be calculated. From the density of liquid nitrogen, they calculate the area per nitrogen molecule as 16.2A^2 and from the solid 13.6A^2, but neither of these can be the correct value to use. One of our objects is to determine the correct values for the different types of solids.

The area of a very finely divided solid in the form of a powder may be determined by a calorimetric method. Due to the fact that our work has been restricted almost entirely to those porous solids of the greatest practical importance at the present time, it has been possible to apply the absolute method to only two materials thus far. These are:

(1) a fine crystalline TiO_2 in the form of anatase, and,
(2) a sample of the same material coated with a small amount of Al_2O_3.

That the *surface* of the latter material is different from that of the former is shown by the fact that the presence of the Al_2O_3 increased very considerably the energy of immersion (E_i) of the material (per unit area) in water.

In order to determine the area of the powder, it is outgassed in a Pyrex tube, connected to another tube which contains a liquid. A smaller tube, which connects those which contain the solid and the liquid, has a transverse glass membrane, which prevents the vapor of the liquid from reaching the solid.

The tube which contains the solid is now sealed off from the vacuum system and placed in a good thermostat (e.g. at 25°C). The membrane is broken and the vapor of the liquid is allowed to come into equilibrium with the surface of the solid. If a large volume of solid is used, glass tubes should lead the vapor to every part of the powder. The attainment of equilibrium *may* require a period of days.

The principal condition to be met is that the liquid chosen for the determination must give a zero angle of contact with the solid. For example, with an unoxidized carbon, a hydrocarbon may be used, while with polar solids water is suitable.

The next step is to immerse the powder, whose particles are coated with a film of the liquid, in a considerable volume of the same liquid in an *extremely* sensitive calorimeter. The amount of heat (q) in ergs per gram, divided by the total surface energy of the liquid (118.5 erg cm^{-2} for water) gives the area per g of powder. Actually there is a correction of the order of one percent for the thickness of the film of liquid.

This method is based upon the idea that the surface of such a duplex film as is formed by adsorption from saturated vapor, and with a zero contact angle, has exactly the surface energy of the liquid itself. With water, the weight of the film indicated a thickness of about 9 molecular layers, while our measurements of energy show that the effect of the solid upon a water film cannot be detected beyond five layers by a calorimetric measurement.

In order to obtain much accuracy by this method, it is essential to have powders with high areas. The powder of highest area gave 13.8 sq. meters per g, while by the use of Emmett's usual assumption of 16.2A^2 for nitrogen, the *BET* method also gave 13.8 sq. meters per g.

[1] S. Brunauer, P. H. Emmett, and E. Teller, J. Am. Chem. Soc. 60, 316 (1938).

A New Adsorption Isotherm Which Is Valid Over a Very Wide Range of Pressure

GEORGE JURA AND WILLIAM D. HARKINS
University of Chicago and Universal Oil Products Company, Chicago, Illinois
July 12, 1943

OIL films on water exist as monolayers in a number of states, such as a two-dimensional perfect and imperfect gas, the liquid expanded state, and several condensed states. The film adsorbed on solids, although not restricted to monolayers, should also exhibit such states. Thus we have found that, in general, the very dilute films are monolayers in the gaseous state, as exhibited by their pressure (π)—area (σ) relations.

Condensed monolayers on water are characterized by the fact that they exhibit the linear pressure-area relation

$$\pi = b - a\sigma \qquad (1)$$

in which a and b are constants and σ is the mean area per molecule.

The pressure-area relations of films on solids had not been determined, but when we plotted them for crystalline powders and porous solids, it was seen that Eq. (1) is valid for condensed films on solids.

The remarkable difference is, however, that the condensed film is monomolecular for only low values of the

film pressure, but *the linear relation persists up to higher pressures where the film is several molecules thick.*

The straight lines were found to be parallel, or almost parallel, so the value of a is constant, or nearly constant, while that of b varies.

Usually there is only one straight line (only one value of a), but in the case of some powders and porous solids, there is a second straight line at higher pressures, which represents a film of greater compressibility. On a charcoal, where the film is almost monomolecular, the compressibility became much smaller at the higher pressures.

Considerable calculation is involved in obtaining the values of the film pressure, so Eq. (1) was transformed into the equivalent relation

$$\log p = B - A/v^2 \tag{2}$$

or,

$$\log (p/p_0) = B - A/v^2, \tag{3}$$

which involves only the quantities p and v which are measured directly in the experimental determination of adsorption.

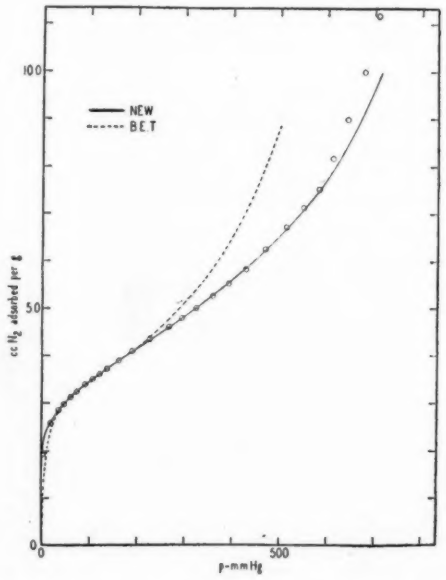

FIG. 1. New and simple *BET* isotherms of N_2 on TiO_2 (anatase).

This equation is remarkable in that (1) it is the simplest adsorption isotherm thus far found; (2) it is valid over more than twice the pressure range of any other two constant adsorption isotherms.

Thus Fig. 1 shows that with TiO_2 in the form of anatase, our new isotherm agrees with the experimental data to both lower and much higher values of pressure than the *BET* isotherm. At very high pressures, both isotherms give too high values for the amount of gas adsorbed, but our curve lies very much closer to the experimental curve.

With porous solids, Fig. 2, our equation seems at low pressures to be somewhat the better of the two, but gives

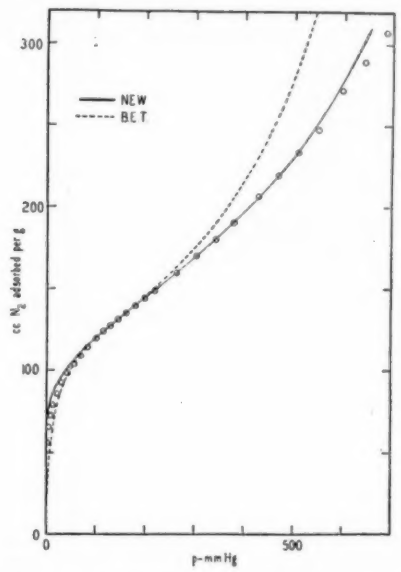

FIG. 2. New and *BET* isotherms of N_2 on a porous solid.

too high amounts, while the *BET* method gives too small amounts, adsorbed. At higher pressures, our isotherm is much the better, but both isotherms give too high values at sufficiently high pressures.

The obvious explanation for this particular deviation of our isotherm is that the smaller capillaries fill up, and prevent the further adsorption which would occur if the pores were sufficiently large. However, the *BET* isotherm gives too high values at the higher pressures even if pores are absent.

An Adsorption Method for the Determination of the Area of a Solid without the Assumption of a Molecular Area, and the Area Occupied by Nitrogen Molecules on the Surfaces of Solids

WILLIAM D. HARKINS AND GEORGE JURA
University of Chicago and Universal Oil Products Company, Chicago, Illinois
July 12, 1943

IN the preceding letter,[1] it was shown that the adsorption isotherm

$$\log p/p_0 = B - A/v^2 \tag{1}$$

is valid over an extremely large range of pressures. This equation represents an S-shaped isotherm.

If $\log p/p_0$ is plotted on the y axis (Fig. 1), (semi-logarithmic paper), a straight line of slope $-A$ is obtained. It is very simple to show that the square roots of the slopes A are proportional to the areas of the solids. Let A be represented by s. Then the area (Σ) for one gram of solid is given by:

$$\Sigma = ks^{\frac{1}{2}} = 4.06s^{\frac{1}{2}}, \tag{2}$$

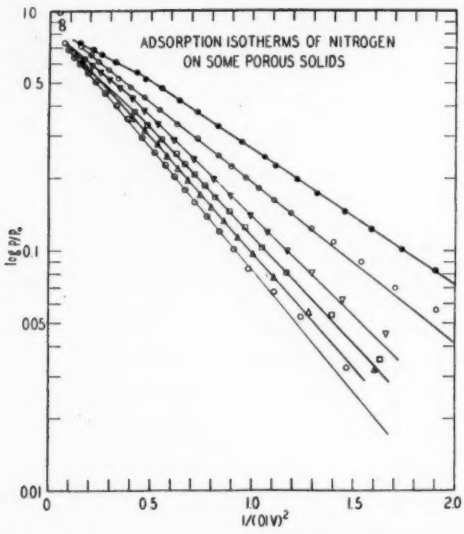

FIG. 1. Adsorption isotherms of nitrogen on some porous solids. These isotherms represent the surfaces of porous solids which have areas, beginning at the top, of 321, 365, 395, 409, 438, and 455 square meters per gram. These areas were determined from these slopes on a large scale plot.

in which Σ is the area in sq. meters per gram if v in Eq. (1) represents the volume adsorbed by 1 g of material.

The value of the constant (4.06) was determined by the substitution in Eq. (2) of the value 13.8 sq. meters per gram for Σ as determined for a sample of anatase by the absolute method described in the first letter. The value of s was determined from the adsorption isotherm of this same powder.

Although the isotherm of Brunauer, Emmett, and Teller is very different from the new isotherm, and although the two were developed from extremely different points of view, the agreement between the values for the area as obtained by the two methods is remarkable. For example, nitrogen was adsorbed on 56 porous and 4 non-porous solids, and the areas were calculated by the use of both isotherms. Since Emmett uses either 13.6A² or 16.2A² as the area per nitrogen molecule, let us choose a value intermediate between the two: 15.25A². If this is done, it is found that for 58 of the sixty solids, the two methods agree to better than ±9 percent.

A more natural method of comparison is obtained if it is remembered that the *BET* method does not give area (Σ) but only the number (N) of molecules to form a complete monolayer, while our method gives the area, but not the number of molecules. So,

$$\sigma = \Sigma / N \qquad (3)$$

gives in each case the mean area (σ) per nitrogen molecule. It is obvious that if this area σ is used in the calculation of area by the *BET* method, the two methods must, of necessity, give identical results.

Thus, from their isotherm, N may be obtained and from ours, Σ, and from the two, the area per molecule of nitrogen on any solid may be calculated. The results of determinations for sixty-one solids are given in Table I.

TABLE I. Area occupied by nitrogen molecules on the surfaces of solids.

Number of solids with N_2 areas between the limits	Area per N_2
1	13.6–13.7
4	13.8–13.9
6 Peak	14.0–14.1
3	14.2–14.3
2	14.4–14.5
1	14.6–14.7
3	14.8–14.9
7	15.0–15.1
9 Peak	15.2–15.3
6	15.4–15.5
2	15.6–15.7
3	15.8–15.9
4	16.0–16.1
5 Peak	16.2–16.3
3	16.4–16.5
0	16.6–16.7
1	16.8–16.9
1	21.3
61	

All of these solids were porous, except four, which gave areas for the nitrogen molecules as follows: anatase 16.1; anatase, sample two, 16.2; anatase coated with Al_2O_3, 16.2; zirconium silicate, 16.4. All of these gave nitrogen areas practically equal to that (16.2) calculated from the density of liquid nitrogen. Other determinations for crystalline powders should be obtained before it is concluded that this is true in general.

It should be noted that only five values fall outside the range of areas calculated from solid (13.6) and liquid (16.2) nitrogen, and three of the five have values of 16.4–16.5 which are almost within this range. It is possible that the single high value (21.3) is erroneous.

It may be noted that the values in Table I give a distribution curve with three peaks, with the highest at an area of 15.25A, the second highest at 14.05, and the lowest at 16.25.

If the relation between $\log p$ and $1/v^2$ is expressed by two straight lines, then that for the *lower* pressures is always taken, since this is the one in which the transition from a monolayer to a polylayer always occurs.

Some porous charcoals have such fine pores that the nitrogen films are restricted to almost a single layer of molecules. For the only charcoal thus far used, our method agreed with that of Langmuir, which gave 1350, while the *BET* method gave 1050 sq. meters per g. In all other cases, our method agrees with the *BET* method, while Langmuir's isotherm was found to be valueless, since it applies only to monomolecular adsorption.

[1] G. Jura and W. D. Harkins, J. Chem. Phys. 11, 430 (1943).

The Configuration of 1,3-Butadiene

R. S. RASMUSSEN, D. D. TUNNICLIFF, AND R. ROBERT BRATTAIN
Shell Development Company, Emeryville, California
July 22, 1943

MULLIKEN[1,2] has calculated the intensity distribution in ultraviolet absorption (1700–2300A) for the *cis-* and *trans-* forms of 1,3-butadiene. Comparison with experimental data[3] indicated that at room temperature the *trans-* form predominates. Rieke and Mulliken[2] made

further calculations on the relative energies of the ground state of the *cis-* and *trans-* forms and concluded that *trans*-butadiene was the lower energy form, although Mulliken indicated that the validity of this conclusion is doubtful because of the approximations used.

Two observations of interest in this connection have been made in these laboratories.

(1) It was found that the ultraviolet absorption of the vapor in the region 2200–2400A is strongly temperature dependent, the optical density increasing with temperature (Fig. 1). The most probable explanation of this effect is

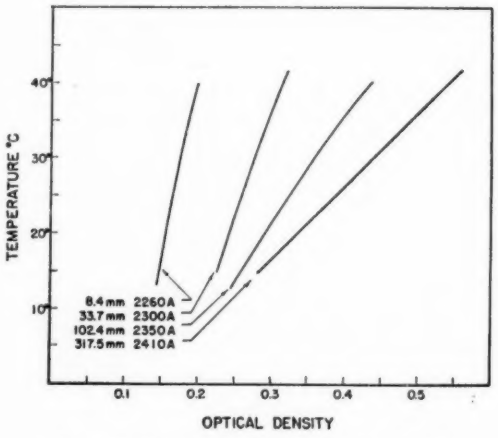

FIG. 1. Optical density of 1,3-butadiene, 1-cm cell.

the existence of appreciable amounts of both isomers at room temperature and a rapidly changing equilibrium in this temperature region. Unfortunately, it was impossible to cover a wide enough temperature range to determine the three parameters governing this temperature dependence, namely, the absorption coefficients of each of the two forms and the energy of isomerization.

(2) A redetermination was made of the infra-red absorption spectrum of the vapor using better resolution and more accurate wave-length calibration than had been used in previously published work.[4,5] The Raman spectrum of the liquid was obtained by Bradacs and Kahovec[6] and was presumably taken at the temperature of a dry ice bath. Of ten infra-red bands and nine Raman lines observed between 1500 and 300 cm.$^{-1}$, six frequencies coincide within the sum of the experimental errors of the two determinations, as shown in Table I. Three of the coincidences occur with the strongest Raman lines in this range. Since the *trans-* form, due to its center of symmetry, should show no coincidences, it is indicated that, under the low temperature conditions of the Raman work, the *cis-* form is predominant. A breakdown of selection rules in the Raman case is not involved, since four coincidences occur with polarized, and hence allowed, Raman frequencies.

TABLE I. Infra-red and Raman frequencies <1500 cm^{-1} of 1,3-butadiene.

Infra-red (vapor) (present work)	Raman (liquid) (Reference 6)
1488(1)	
1432(1)	1437(4) *P*
1383(5)	
1302(1)	1303(2) *P*
1273(3)	1276(4) *P*
	1200(4) *P*
1014(9)	1025(0)
988(2)	
909(10)	914(2) *D*
	899(1) *D*
665(1)*	
520(5)*	513(4) *P*
	340(00)

* Taken from reference 4. Raman polarizations and approximate Raman and infra-red intensities shown.

From the foregoing observations and considerations it appears that *cis*-butadiene is the lower energy form. The *cis-* form predominates at the temperature of a dry ice bath, while at room temperature the *trans-* form predominates, as indicated by the ultraviolet spectrum, although a considerable proportion must be in the *cis-* form in order to account for the coincidences of the infra-red spectrum observed at room temperature and the Raman spectrum observed at the lower temperature.

[1] R. S. Mulliken, J. Chem. Phys. **7**, 121 (1939).
[2] R. S. Mulliken, Rev. Mod. Phys. **14**, 269 (1942).
[3] E.g., see E. P. Carr, L. W. Pickett, and H. Stücklen, Rev. Mod. Phys. **14**, 260 (1942).
[4] E. Bartholomé and J. Karweil, Zeits. f. physik. Chemie **B35**, 448 (1937).
[5] R. B. Barnes, U. Liddel, and V. Z. Williams, Ind. Eng. Chem. Anal. Ed. **15**, 83 (1943).
[6] K. Bradacs and L. Kahovec, Zeits. f. physik. Chemie **B48**, 63 (1940).

THE AMERICAN INSTITUTE OF PHYSICS

INCORPORATED

ADMINISTRATIVE STAFF

HENRY A. BARTON, *Director*

MADELINE M. MITCHELL, *Publications Manager*

JOHN T. TATE, *Adviser on Publications*

Office: 175 Fifth Avenue, New York 10, New York

JOURNALS

THE PHYSICAL REVIEW
REVIEWS OF MODERN PHYSICS
JOHN T. TATE, *Editor (on leave)*
J. W. BUCHTA, *Acting Editor*

JOURNAL OF THE OPTICAL SOCIETY OF AMERICA
GEORGE R. HARRISON, *Editor*

THE JOURNAL OF THE ACOUSTICAL SOCIETY OF AMERICA
FLOYD A. FIRESTONE, *Editor*

AMERICAN JOURNAL OF PHYSICS
DUANE ROLLER, *Editor*

THE REVIEW OF SCIENTIFIC INSTRUMENTS
GAYLORD P. HARNWELL, *Editor*

THE JOURNAL OF CHEMICAL PHYSICS
JOSEPH E. MAYER, *Editor*

JOURNAL OF APPLIED PHYSICS
ELMER HUTCHISSON, *Editor*

GOVERNING BOARD

PAUL E. KLOPSTEG, *Chairman*
Central Scientific Company

GEORGE B. PEGRAM, *Secretary*
Columbia University

For the American Physical Society:

JOHN T. TATE
University of Minnesota

L. A. DUBRIDGE
University of Rochester

GEORGE B. PEGRAM
Columbia University

For the Optical Society:

A. C. HARDY
Massachusetts Institute of Technology

K. S. GIBSON
National Bureau of Standards

R. C. GIBBS
Cornell University

For the Acoustical Society of America:

HARVEY FLETCHER
Bell Telephone Laboratories

FLOYD A. FIRESTONE
University of Michigan

WALLACE WATERFALL
The Celotex Corporation

For the Society of Rheology:

R. B. DOW
Aberdeen Proving Ground

HERMANN MARK
Brooklyn Polytechnic Institute

N. W. TAYLOR
The Pennsylvania State College

For the American Association of Physics Teachers:

A. G. WORTHING
University of Pittsburgh

PAUL E. KLOPSTEG
Central Scientific Company

T. D. COPE
University of Pennsylvania

The American Institute of Physics is a membership corporation of which five societies are the founding members. These five societies are the principal national societies devoted to pure and applied physics in America. Their names, and those of their representatives who form the Governing Board of the Institute, are given above. The principal work of the Institute is the publication of journals sponsored by the societies or by itself. The names and the editors of the journals are also listed above.

The broad purpose of the Institute is to represent, in all matters of wide or common interest, the five thousand or more members and subscribers associated with the Founder Societies and the journals. It aims to advance the science and profession of physics, and to promote cooperation between pure research, the applied sciences and the industries. To achieve these aims, it is greatly in need of an endowment and is empowered by law to administer grants and funds of any kind.

CONTENTS

THE JOURNAL OF CHEMICAL PHYSICS VOL. 11, NO. 9 SEPTEMBER, 1943

Equilibrium in Hydrogen-Water Systems Containing Tritium . . . . . JAMES F. BLACK AND HUGH S. TAYLOR 395

Use of the Exchange Between Carbon Dioxide, Carbonic Acid, Bicarbonate Ion, and Water for Isotopic Concentration . . . . . ALLEN F. REID AND HAROLD C. UREY 403

Photographic Latent Image. I. Lattice Energy and Related Quantities for a Hypothetical Silver Bromide Crystal Having the Cubic ZnS Type of Structure . . . MAURICE L. HUGGINS 412

Photographic Latent Image. II. Outline of the Theory . . . . . MAURICE L. HUGGINS 419

X-Ray Diffraction Investigation of Sodium Stearate from Room Temperature to the Melting Point . . . . . A. E. BEETEVILLE, JR., AND J. W. MCBAIN 426

Letters to the Editor:

Absolute Method for the Determination of the Area of a Fine Crystalline Powder . . . . . WILLIAM D. HARKINS AND GEORGE JURA 430

New Adsorption Isotherm Which is Valid over a Very Wide Range of Pressure . . . . . GEORGE JURA AND WILLIAM D. HARKINS 430

Adsorption Method for the Determination of the Area of a Solid Without the Assumption of a Molecular Area, and the Area Occupied by Nitrogen Molecules on the Surfaces of Solids . . . . . WILLIAM D. HARKINS AND GEORGE JURA 431

Configuration of 1,3-Butadiene R. S. RASMUSSEN, D. D. TUNNICLIFF AND R. ROBERT BRATTAIN 432

LANCASTER PRESS, INC., LANCASTER, PA.